NASA LaRC Hypersonic Experimental Aerothermodynamic Capabilities and Recent Contributions

Michelle L. Mason[*], Shann J. Rufer[†], Brian R. Hollis[‡], Scott A. Berry[‡], Gregory M. Buck[†], Victor R. Lessard[*], F. Drew Turbeville[§], Matthew N. Rhode[*], Jonathan S. Cheatwood[**], Neil S. Rodrigues[††], Brett F. Bathel[‡‡], Andrew N. Leidy[§§]

NASA Langley Research Center, Hampton, VA 23681

A review is presented of recent research efforts that were conducted at the NASA Langley Research Center in the Langley Aerothermodynamics Laboratory. An overview of the test facilities, model development and fabrication capabilities, and instrumentation and measurement techniques employed in this work is provided. Contributions to hypersonic flight and planetary exploration programs are detailed, as are fundamental research and development activities. Wind tunnel investigations that supported flight programs for NASA are described herein. Collaborations between NASA projects and academia are also highlighted in this overview of recent wind tunnel experimental campaigns.

I. Introduction

NASA Langley Research Center (LaRC) provides experimental aerothermodynamic support to Agency hypersonic flight programs. This portfolio has included the Gemini-Mercury-Apollo space race and the Space Shuttle development, the previous and current Mars exploration programs, and numerous planetary reentry missions. Recently, the Langley Aerothermodynamics Laboratory ground test facilities supported NASA flight programs such as Artemis, the Low-Earth Orbit Flight Test of an Inflatable Decelerator (LOFTID), and the Mars Sample Return mission.

The NASA LaRC experimental contributions and lessons learned in support of recent national and agency hypersonic flight initiatives are presented by category of flight program support, academic partnerships, foundational research and development, test technique development, and facility calibrations. Hollis et al. [1] and Berry et al. [2] previously provided a similar review of experimental accomplishments and contributions for blunt reentry configurations and slender to moderately blunt lifting body configurations, respectively. The current compilation of recent testing activity covers the spectrum of blunt to lifting body configurations. The scope for the present review is

[*] Aerospace Engineer, Aerothermodynamics Branch, Research Directorate, AIAA Senior Member

[†] Aerospace Engineer, Aerothermodynamics Branch, Research Directorate, AIAA Associate Fellow

[‡] Senior Technical Lead, Aerothermodynamics Branch, Research Directorate, AIAA Associate Fellow

[§] Aerospace Engineer, Aerothermodynamics Branch, Research Directorate, AIAA Member

[**] Aerospace Engineer, Aerothermodynamics Branch, AIAA Student Member

[††] Optical Physicist, Advanced Measurements and Data Systems Branch, AIAA Member

[‡‡] Aerospace Engineer, Advanced Measurement & Data Systems Branch, Research Directorate, AIAA Senior Member

[§§] Research Aerospace Engineer, Flow Physics and Control Branch, Research Directorate, AIAA Senior Member

limited to recent (2017-2024) significant aerothermodynamic impacts from experimental studies conducted in the Langley Aerothermodynamic Laboratory (LAL).

The discipline of aerothermodynamics blends aerodynamics, aeroheating, and fluid dynamics to provide essential environmental information for advanced space transportation and transatmospheric vehicles. A hypersonic vehicle design cycle requires synergistic feedback between the disciplines of aerothermodynamics, structures, materials, propulsion, avionics, and guidance, navigation, and control. Hypersonic experimental facilities are necessary to advance national interests of space access and military supremacy. Ideally, data from ground-based testing, computational fluid dynamics (CFD) predictions, and flight experiments provide a triad of capabilities to characterize the aerothermodynamic environments for high-speed, access-to-space, and entry, descent, and landing vehicles. Wind tunnels provide the capability to quickly screen preliminary vehicle configurations, develop flight databases and/or validate CFD wind tunnel simulations of full vehicle designs. Validated CFD models are applied to compile a comprehensive, parametric database of laminar and turbulent environments at points of interest along a trajectory. When the schedule and budget of a project permit, targeted flight experiments verify the functionality of the final design prior to deeming a vehicle or subsystem operational. By utilizing all three approaches for aerothermodynamic design, each individual component of the triad can be reinforced and strengthened through final comparisons of the extracted flight performance data to wind tunnel simulations and CFD predictions.

Historically, the LAL facilities operated nearly continuously in support of numerous test programs except for scheduled maintenance downtime. However, in the late 2000s, NASA shifted to a full-cost accounting model. The test facilities were no longer treated as Agency-level assets funded at a top-level; instead, customers were charged at much higher rates for their wind tunnel entries, leading to a reduction in the number of test programs. The trend was reversed in 2017 when NASA's Aerosciences Evaluation and Test Capabilities (AETC) office introduced a funding model that drastically reduced the customer occupancy costs. The new model led to increased demand for testing, including foundational and applied research, collaborations with universities on fundamental problems, agreements with external defense and industry partners, and support for NASA missions.

The trend of increasing tunnel utilization is shown in Fig. 1, which also includes a notable gap in 2020-2021 when on-site access to NASA centers was limited due to the COVID-19 pandemic. LAL testing through May in fiscal year (FY) 2024 is captured in the plot; the dashed rectangle represents the predicted runs in the LAL queue for the remainder of that FY. The 20-Inch Mach 6 Air Tunnel was the workhorse facility during this time; the 31-Inch Mach 10 Air Tunnel will soon resume customer testing after a lengthy downtime for various repairs. Together, the LAL facilities provide flexible, low-cost hypersonic test capabilities that no other national facilities match, as evidenced by the current backlog of testing.

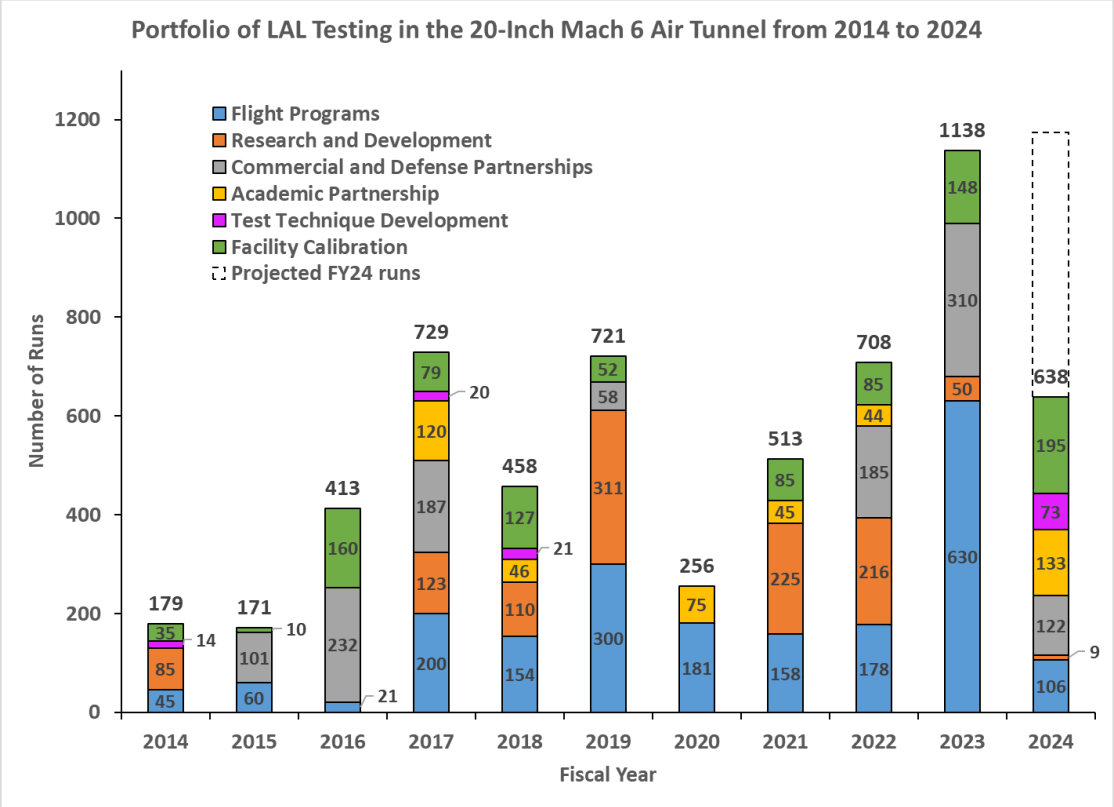

Fig. 1 Decade of recent testing in the LAL 20-Inch Mach 6 Air Tunnel.

II. Review of LAL Facilities and Capabilities at NASA LaRC

The LAL consists of the 20-Inch Mach 6 and the 31-Inch Mach 10 tunnels, pictured in Fig. 2, as well as a 60-foot vacuum sphere (not described in this paper). Both tunnels are conventional blow-down hypersonic facilities that use dried, filtered, and heated air as the test gas and provide for a range of freestream unit Reynolds numbers, Re_∞, and normal shock density ratios, ρ_2/ρ_∞. The tunnel names define the free-stream Mach numbers, M_∞. The LAL facilities can conduct proprietary, controlled unclassified information (CUI), International Traffic in Arms Regulation (ITAR), and classified tests. Detailed descriptions of these facilities and a historical perspective on their operation, maintenance, and upgrades can be found in Ref. 3.

Information on all the NASA wind tunnels across the speed range at Langley (and other centers) can be found at the NASA Aeronautics Program website http://www.aeronautics.gov/atp. Recent tests conducted in the LAL 20-Inch Mach 6 Air Tunnel and the 31-Inch Mach 10 Tunnel are discussed in this paper.

The NASA LaRC Aerosciences Operations Section conducts tunnel operations and provides technical support for data acquisition in the LAL facilities. Principle Investigators who develop, lead and conduct test campaigns are drawn from the LaRC Aerothermodynamics, Flow Physics and Control, Advanced Measurement & Data Systems, and Atmospheric Flight & Entry Systems Branches, depending on the programmatic objectives and required test techniques. Collectively, this group of researchers comprises the Langley Experimental Aerothermodynamics Discipline team. Computational fluid dynamics support for both pretest planning and post-test comparison/validation exercises is provided by computational experts from the Aerothermodynamics, Atmospheric Flight & Entry Systems and/or the Computational Aerosciences Branches.

NASA LaRC 31-Inch Mach 10 Air Tunnel

NASA LaRC 20-Inch Mach 6 Air Tunnel

[Photos source: NASA]

Fig. 2 Langley Aerothermodynamic Laboratory (LAL).

A. 20-Inch Mach 6 Air Tunnel

The 20-Inch Mach 6 Air Tunnel (Fig. 3) is a thermally perfect-gas, blow-down facility that uses dried, filtered air as the working fluid. This tunnel shares pressure and vacuum infrastructure with other facilities on center. The tunnel has been calibrated for reservoir conditions varying from 30 psia to 475 psia at operating temperatures from 760 °R to 940 °R, which produce freestream unit Reynolds numbers from 0.5×10^6/ft to 8.0×10^6/ft at Mach numbers from 5.75 to 6.05. The 2-D planar nozzle has parallel sidewalls bounding the contours that expand from a 0.399-in. × 20-in. throat. The 20.5-in. × 20-in. test section has a core size approximately 12 inches to 14 inches across, depending on Reynolds number. Optical access is provided through windows on the top and sides. The injection system is bottom mounted with a -5° to +55° pitch range and ±10° yaw range. With a wide Reynolds number range capable of producing laminar, transitional, and turbulent flow on a model, the tunnel is primarily used for heat-transfer and boundary-layer transition studies.

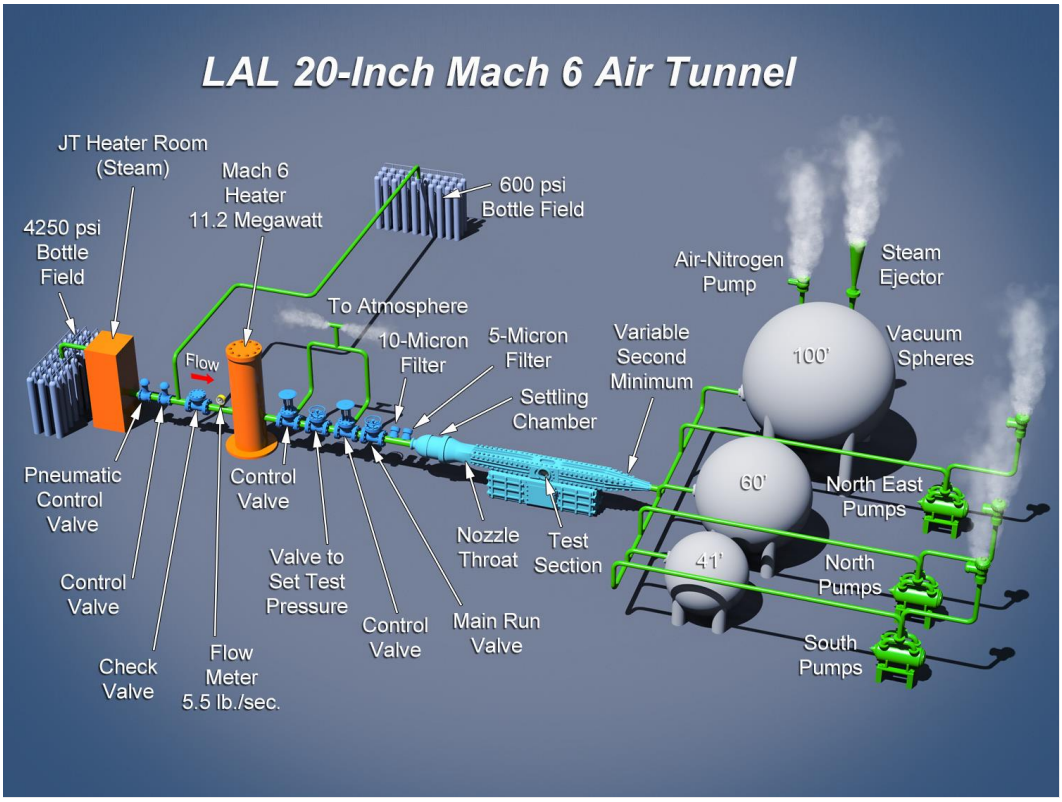

Fig. 3 LAL 20-Inch Mach 6 Air Tunnel.

B. 31-Inch Mach 10 Air Tunnel and 15-Inch Mach 6 Air Tunnel

The 31-Inch Mach 10 Air Tunnel (Fig. 4) is a thermally perfect-gas, blow-down facility that uses dried, filtered air as the working fluid. The tunnel has been calibrated for reservoir conditions varying from 150 psia to 1450 psia at an operating temperature of 1850 °R, which produces freestream unit Reynolds numbers from 0.25×10^6/ft to 2.2×10^6/ft. The nozzle is water-cooled and has a three-dimensional (3-D) contour that expands from a 1.07-in. square throat. The 31-inch square test section features optical access through side, top, and bottom windows for visual imaging techniques and has a side-mounted injection system with a -45° to +45° pitch range and ±5° yaw range. The test core varies from approximately 12 inches × 12 inches at the lowest Reynolds number to 14 inches × 14 inches at the highest Reynolds number. This tunnel is utilized for aerodynamic, aerothermodynamic, and basic fluid dynamic studies (e.g., boundary layer and laminar-to-turbulent transition). The high stagnation temperature of the facility also makes the 31-Inch Mach 10 Air Tunnel suitable for aftbody/wake heating studies where heating rates are much lower than those on the forebody and are more difficult to measure accurately.

The 15-Inch Mach 6 Tunnel is a separate test leg off the 31-Inch Mach 10 tunnel that shares the same high-pressure air and vacuum systems but has an independent control room and data acquisition systems. This facility has a walk-in, open-jet test section approximately 6 feet long, 6 feet wide and 7.25 feet high. The flow exhausts into this vacuum chamber, traverses the model test area, and is collected approximately 18 inches downstream of the nozzle exit into a variable area diffuser equipped with an adjustable second minimum and a water-cooled heat exchanger. Models are supported on a hydraulically-operated, injection/retraction support mechanism that provides a pitch angle range of -10° to +50° and yaw angles between ±10°. The tunnel is equipped with numerous optical access ports, including three 29 in. x 23 in. windows on each side and on the top of the tunnel and four 5.5-in. diameter circular windows (two on each side) located approximately 45° above the model. The 15-Inch Mach 6 Tunnel rarely operates as a hypersonic testing facility; rather, this facility is used primarily as a vacuum chamber for reaction control system (RCS) nozzle calibrations or instrumentation development.

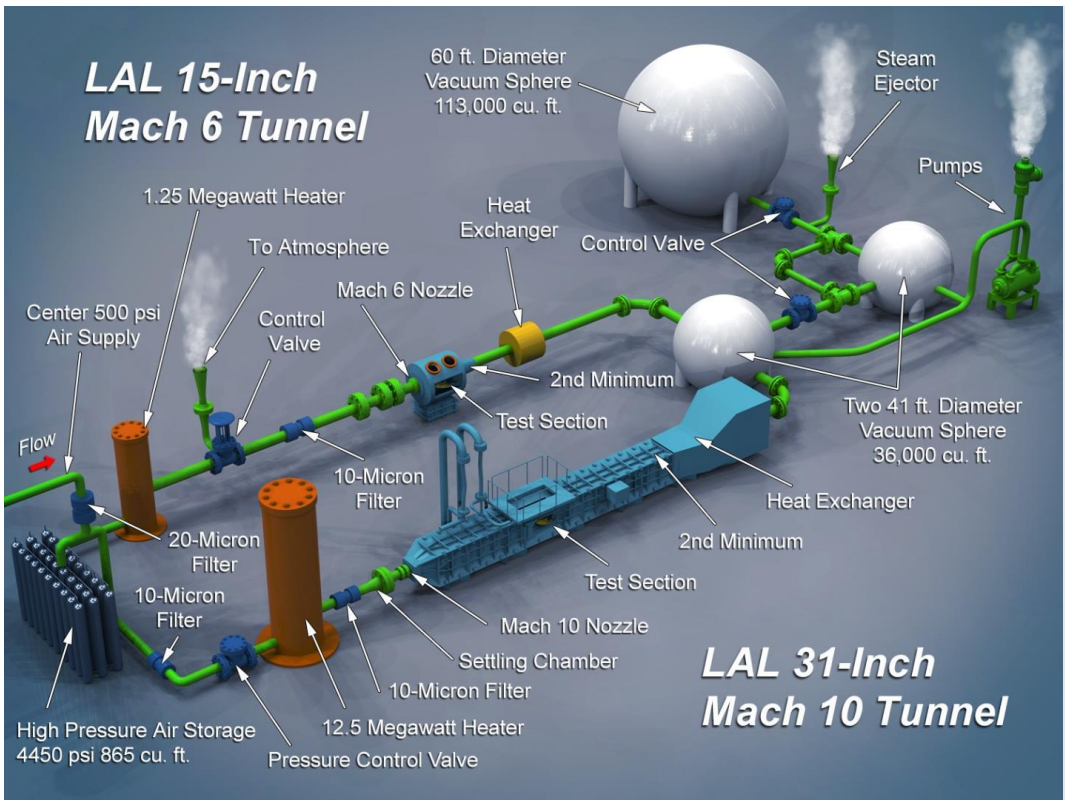

Fig. 4 LAL 31-Inch Mach 10 Air Tunnel and 15-Inch Mach 6 Air Tunnel.

C. Test Techniques

Measurement capabilities available in the LAL facilities include a variety of global and discrete surface heat-transfer techniques, mean and fluctuating surface pressure measurements, aerodynamic force-and-moment measurements – including stage-separation and RCS interactions, and flowfield visualization and characterization. Customer-developed measurement techniques also may be employed during testing.

1. Global Optical Surface Heat-Transfer Techniques

Global optical surface thermography techniques are employed in most LAL test programs to generate heat-transfer data. These techniques include phosphor, infrared, and temperature-sensitive paint thermography. Each of these techniques provides orders of magnitude more data (i.e., image pixels) than discrete sensor measurements. Global techniques provide both heating and temperature time-history data. Contour maps of the model surface data acquired with these methods are ideally suited for locating flow features such as boundary-layer transition and shock-shock or shock-wave-boundary-layer interactions. Rapid, in-house fabrication of wind tunnel models for thermography methods through ceramic casting [4] and/or 3D printing permit low-cost testing of multiple vehicle configuration parameters with features on the order of 0.005". For test programs with requirements for finer model surface features, such as sharp nose tips or leading edges, metallic models also may be fabricated either in-house or through external contractors.

Data processing is similar for each of the optical thermography techniques described below. Optical signals are recorded and converted to temperatures, and then temperature-time histories are used to compute heating rates. The data product of these techniques are two-dimensional, image-pixel maps of temperature and heating. The 2D images can be further manipulated through extraction of profile lines at specified stations, as well as processed through optical

translation, rotation, scaling, and perspective transformations to map the images onto 3D surface CAD representations of a wind tunnel model.

The Imaging for Hypersonic Experimental Aeroheating Testing (IHEAT) program, a one-dimensional, semi-infinite domain heat-flux conduction code [5], is the primary tool for processing global thermography data. IHEAT was originally developed for use with the phosphor thermography technique, but modules for processing both infrared and temperature sensitive paint data have been developed and are being validated. Updates to the IHEAT thermal analysis algorithm are underway to incorporate multi-dimension conduction, three-dimensional mapping to CAD surfaces, speed improvements, and other features.

Two-Color, Relative Intensity Phosphor Thermography: Phosphor thermography [6, 7] uses cast-ceramic wind tunnel models coated with a mixture of rare-earth compounds that fluoresce under ultraviolet (UV) stimulation. Pre-test, laboratory calibrations provide a temperature-dependent emission intensity response function of the phosphor mixture. Phosphor emissions are recorded via a three-color CCD camera and the relative intensity ratio of red and green channels is used to eliminate any response variance due to incident illumination levels.

In the wind tunnel, the phosphor-coated ceramic models are illuminated by UV lights and an intensity versus time history is recorded from an ambient, pre-run condition through the duration of a run. The intensity-time history is then converted to a temperature-time history through the calibration, and then a heating-time history is calculated through a heat-conduction analysis.

Phosphor thermography has been the primary heat-transfer technique used in the LAL wind tunnels over the last 30 years because it is a fast, accurate and inexpensive method with a wide range of applications. However, phosphor thermography is not ideal in conditions where either very low (e.g., wake flows) or very high (e.g., shock-shock interactions at a high Reynolds number) model surface temperatures are produced. Additionally, while not a limitation of phosphor thermography itself, the use of cast ceramic models with the technique limits testing of some configurations with very fine surface features such as sharp leading edges. For such applications, either infrared or temperature sensitive paint thermography may be employed.

Infrared (IR) Thermography: In IR thermography [8], temperature-dependent IR emissions from a wind tunnel model are recorded, converted from signal counts to temperatures, and then processed to determine a heating-time history. IR thermography may be employed with machined, 3D printed or ceramic cast models, but is optimal for use with model materials that have a low thermal conductivity and high emissivity with minimal thermal reflectivity. The use of precision-machined models with IR thermography provides the capability for resolution of finer features than that of cast ceramic models employed with phosphor thermography.

Historically, IR thermography has rarely been used in the LAL facilities due to the ease and general applicability of phosphor thermography. However, over the last 5 years, several pathfinder studies have been conducted to evaluate the use of IR thermography. Efforts are now underway to develop IR thermography into a fully-operable, “turn-key” system for regular use in the LAL. Upgraded hardware have been procured including high-resolution mid-wavelength cameras, calibration sources, and broad-bandwidth tunnel windows. The operational implementation of IR will enable highly accurate and spatially-resolved surface heat-flux measurements that are corrected for directional emissivity and ambient reflections.

Temperature-Sensitive Paint (TSP) Thermography: In the TSP technique [9], polymer mixtures comprised of luminescent molecules are applied (painted) on the surface of a wind tunnel model and the optical response over time is recorded, converted to temperature and then to heat-transfer. TSP compounds are optimized for low temperature response and are thus most frequently employed in sub / trans / supersonic test facilities where lower heating rates are produced. TSP does have applications in hypersonic facilities such as the LAL for situations like the aftbody of a blunt capsule [10] in which the separated wake flow results in low temperature and low heating conditions. The TSP formulation may be adjusted to target pressure changes instead of temperature, resulting in a global pressure-sensitive paint (PSP) capability, which is also available for use in the LAL.

2. Discrete Surface Measurement Techniques

Discrete surface temperature and heat-flux measurement techniques, including thin-film resistance heat-flux gauges, coaxial surface thermocouples, and thin-skin calorimeter gauges, also may be used for temperature and heating data acquisition in the LAL tunnels. Discrete sensors have been used in a limited sense due to their greater cost, increased fabrication complexity, and lower data quantity output compared with the global techniques. However, discrete sensors are critical for certain applications, such as model geometries where heating data is required in regions with no optical field-of-view or for flow-fields in which high-frequency response measurements are desired. Examples of applications of these sensors are documented in Refs. 11-13. Discrete sensor data are processed using methods described in Ref. 14 through the One-Dimensional Hypersonic Aero-Thermodynamic (1DHEAT) data reduction code [15] to obtain heat-transfer rates.

Discrete surface pressure instrumentation techniques can be used to measure static and high-frequency, fluctuating surface pressures in the LAL tunnels. Electronically-scanned pressure (ESP) transducer modules are typically used for mean measurements and PCB® piezoelectric transducers or Kulite® piezoresistive transducers are used for dynamic measurements (e.g., Ref. 16).

3. Aerodynamic Force and Moment Measurements

Aerodynamic loads on test articles in the LAL are typically measured using internally mounted, six-component, strain-gage balances to obtain three forces (axial, side, and normal) and three moments (roll, pitch, and yaw). The balances utilize integral water-cooling jackets to maintain thermal stability during testing, with temperatures at the forward and aft strain gage locations measured using thermocouples or platinum resistive thermometers (PRT) to assess longitudinal thermal gradients during a run. Additionally, the measured balance voltages are temperature-compensated via the internal wiring up to a temperature of 180 °F.

Most aerodynamic tests are performed using a single balance in a single test article. The instrumentation, data acquisition, and data reduction systems are capable of handling multiple balances simultaneously, such as to characterize aerodynamic interactions between separating bodies [17].

Water-cooled, five-component (no axial force), flow-through balances are used for loads measurements while simulating propulsive effects from RCS or forward-firing retro-propulsion systems. A high-pressure tube runs through the center of the balance to supply a simulant gas (typically air or nitrogen) to the model plenum and propulsive nozzles. RCS aerodynamic jet interaction measurements are often coupled with flowfield diagnostics to measure the shape and size of nozzle plumes and surface interaction regions.

Force balance measurements are acquired using either move-pause or continuous-sweep data acquisition methods. For the latter, the model is moved in either pitch or yaw at a constant angular rate (typically 1 to 2 deg/sec) while recording data at a specified sampling rate. The introduction of continuous-sweep data acquisition in the LAL facilities has significantly increased test productivity and data volume for aerodynamic testing.

Temperature-compensated piezoresistive pressure transducers often are used for base and sting-cavity pressure measurements to greatly reduce or eliminate pneumatic lag associated with the low freestream static pressures in the LAL facilities.

4. Flowfield Diagnostics and Visualization Techniques

Flowfield measurement techniques including focusing schlieren, zoom schlieren, background-oriented schlieren, and other schlieren systems are utilized to visualize density gradients that are ubiquitous with high-speed aerodynamics, e.g., shock structures, flow separation, and boundary layers. A variety of planar laser-induced fluorescence (PLIF) techniques [18, 19] can be employed to obtain velocimetry information on flowfield features such as boundary layers or expanding RCS plumes. Pressure surveys are performed using pitot probes to measure both the time-averaged flow uniformity [20] and fluctuations [21], which can contribute to boundary-layer transition on a model.

Near-surface flow velocities are visualized through an oil flow technique that involves coating black, smooth models with oils of various viscosities (depending on expected surface shear levels) combined with white pigment. Shear forces at the surface cause the oil to move or coalesce along near-surface streamline patterns. Important features like shock impingements, flow separation and reattachment lines can be defined using this technique.

D. Synergy with In-House Computational Capabilities

Expertise in computational simulations across the regime of continuum sub / trans / super / hyper sonic flow and low-density rarefied flow resides in multiple organization at NASA LaRC, including the Aerothermodynamic Branch, which conducts the majority of LAL testing. Computational capabilities relevant to LAL conditions include the Langley Aerothermodynamic Upwind Relaxation Algorithm (LAURA) and the Fully Unstructured in Three Dimensions (FUN3D) flow field solvers and the Langley Stability and Transition Analysis Code (LASTRAC) boundary-layer stability code.

The LAURA code [22, 23] is a three-dimensional, finite-volume, structured grid topology Navier-Stokes solver for hypersonic flows, which incorporates perfect-gas, equilibrium chemistry, and nonequilibrium reacting gas thermodynamic options, as well as a variety of turbulence models and coupled ablation and radiation transport models. The FUN3D code [24] is a three-dimensional, finite-volume, unstructured grid topology Navier-Stokes solver for continuum sub / super / hyper sonic flows. FUN3D incorporates perfect-gas and equilibrium air models and shares the nonequilibrium reacting gas thermodynamics models implemented in LAURA. FUN3D includes adjoint-based error estimation and grid adaption which permit more efficient computations of complex vehicle topologies and flow fields. With greater accuracy in the prediction of surface heating distributions, LAURA is more commonly used for aeroheating simulations, while either LAURA or FUN3D are used for aerodynamic simulations. For both codes, a perfect-gas model is employed for simulations of LAL flow conditions, with either laminar or turbulent boundary-layer models, as appropriate.

For a more specialized application of boundary-layer transition prediction, the LASTRAC stability code [25] can be used in conjunction with experimental studies. LASTRAC uses both quasi-parallel linear stability theory (LST) and Parabolized Stability Equations (PSE) for stability analysis and N-factor growth mapping to predict the onset of boundary-layer transition.

These computational tools and experimental studies combine to provide pre-test assistance in test program development. Post-test computational comparisons with experimental data facilitate the development of combined experimental-computational models for aerothermodynamic phenomena such as boundary-layer transition, heating augmentation due to discrete features (such as protrusions, steps, or cavities), aerodynamic / RCS interaction effects, etc. This joint experimental-computational approach permits computational model validation, CFD definition of parameters for correlation or to scale the experimental data to flight conditions, and the application of computed flow field properties to interpret the flow physics (e.g., shock structures and interactions, boundary-layer separation and reattachment, sonic-line location, etc.) that produce the properties that are measured experimentally.

III. Flight Programs

LAL hypersonic wind tunnels extensively support NASA missions and programs as well as external defense, commercial, and academic customers. Customers receive LAL data in the form of aeroheating images and line profiles generated via phosphor and IR thermography, aerodynamic force-and-moment coefficients, and flow field visualizations, as appropriate. These data are used to perform initial vehicle configuration screening, flight database development or computational validation exercises. LAL tests that contributed to recent flight programs are described in the following subsections.

A. Orion Multi-Purpose Crew Vehicle

The Orion Multi-Purpose Crew Vehicle (MPCV), previously known as the Crew Exploration Vehicle (CEV), is an Apollo-like capsule NASA developed as a reentry vehicle for human deep space exploration missions to the Moon

and beyond. Although Orion shares a clear heritage with the Apollo capsule design, such as an Avcoat thermal protection system (TPS), the Orion MPCV is considerably larger, which results in higher heating rates and aerodynamic loads, and features some geometric differences, mainly in the shape of the crew compartment.

Multiple entries in the LAL tunnels (see [26,27]) were performed in support of the Orion capsule development before the Exploration Flight Test (EFT-1) mission in 2014, which was an uncrewed demonstration of vehicle performance at orbital return velocity. After EFT-1, the original monolithic heat shield was replaced with a design that incorporates multiple, conformally molded blocks, similar to the design of the Mars Science Laboratory entry vehicle [26]. Gaps between these blocks are filled with a room-temperature-vulcanizing (RTV) silicone. Since the RTV filler and Avocat TPS can ablate at different rates, the potential exists for either gaps or "fences" of RTV to form between the blocks. These steps and gaps can affect both boundary-layer transition and surface heating levels and were not accounted for in the original Orion EFT-1 database. To support the development of a new database on the blocked TPS design, several entries were made in the LAL wind tunnels to obtain boundary-layer transition and aeroheating data in support of the subsequent Artemis-I mission to demonstrate the system's performance at super-orbital (i.e., lunar return) conditions.

These ground tests provided critical traceability-to-flight information to support the Artemis I mission. Specifically, these tests contributed to the risk assessment for a combined aerothermal environment and TPS ablation coupling by verifying the block Avcoat RTV fence induced laminar-to-turbulent boundary-layer transition assumptions.

1. Pathfinder study using IR Thermography for Orion blocked TPS data acquisition

To support investigations of the new blocked-TPS design, an initial pathfinder study was conducted in the 20-Inch Mach 6 and 31-Inch Mach 10 Air Tunnels to evaluate several changes to previous Orion aeroheating test methodology at LAL. At that time, the capability for fabricating ceramic models placed limitations on the scale of small model features (e.g., blocked TPS steps and gaps), so the option of using precision-machined models from polyether ether ketone (PEEK) was evaluated for thermography testing. The PEEK heat-transfer data were obtained using the developmental IR thermography technique instead of standard phosphor thermography due to the different thermal and optical response properties of PEEK. Phosphor thermography data also were obtained using conventional, cast-ceramic models as a comparison standard to the IR data with PEEK models. The PEEK models featured variable fence heights ranging from 0.018" down to 0" (smooth). The cast-ceramic models were made from plastic resin molds printed using a stereo-lithography apparatus (SLA) which could only produce fence heights in the range of 0.005" to 0.010". Since this study, the use of higher-precision 3D wax printed model patterns in place of SLA resin printing has improved ceramic model resolution to feature sizes on the order of about 0.003" to 0.005". Additionally, "zoomed" views of the block-TPS were evaluated to provide higher resolution of the small fence and gap features.

Sample phosphor thermography results using ceramic models are shown in Fig. 5 and sample IR thermography results using PEEK models are shown in Fig. 6. The successful pathfinder study demonstrated the utility of machining and testing PEEK models, albeit at a higher cost and longer lead time than casting ceramic models. The IR thermography data was deemed to be qualitative as further analysis of the results highlighted several issues to address to bring this technique to a quantitative, operational status. These steps included evaluating PEEK's thermal properties and optical directional emissivity characteristics, acquiring dedicated IR cameras for future testing (since borrowed cameras were employed for this test) and validating the reduction and analysis methods used for IR thermography. All these improvements are currently being worked by the LaRC research team.

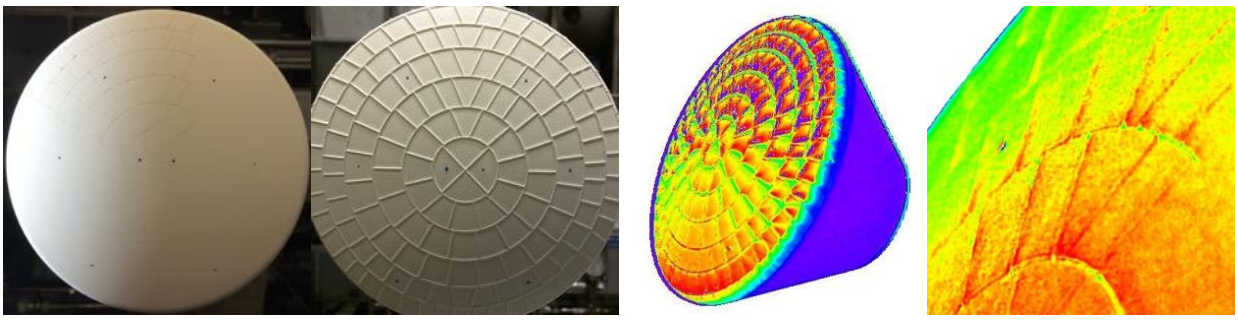

Fig. 5 Phosphor thermography data on ceramic Orion models tested in the 31-Inch Mach 10 Air Tunnel. [Photos Source: NASA]

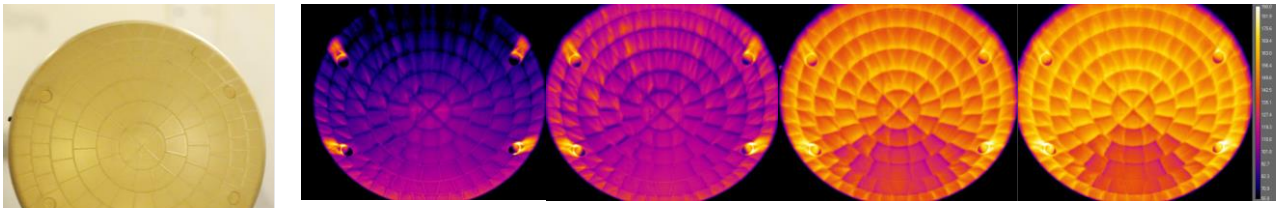

a) Re = $1x10^6$/ft b) Re = $2x10^6$/ft c) Re = $4.8x10^6$/ft d) Re = $6.2x10^6$/ft

Fig. 6 IR thermography data on PEEK Orion models tested in the 20-Inch Mach 6 Air Tunnel [Photo Source: NASA].

2. TPS Fences and Heatshield Recession using IR Thermography

After the pathfinder test demonstrated the capability to use precision-machined models with IR thermography, a dedicated test program was conducted to obtain aeroheating data on configurations both with fences between the TPS blocks and with simulated post-flight recession patterns on the heatshield. Sample data from the test program are shown in Fig. 7. These tests and comparisons with results from flight testing demonstrate the traceability and applicability of ground test data to flight conditions. These data helped demonstrate that physics models for boundary-layer transition and heating augmentation, developed from simulations and ground testing, were conservative, which retired some of the mission risks carried by the project prior to the Artemis-I launch.

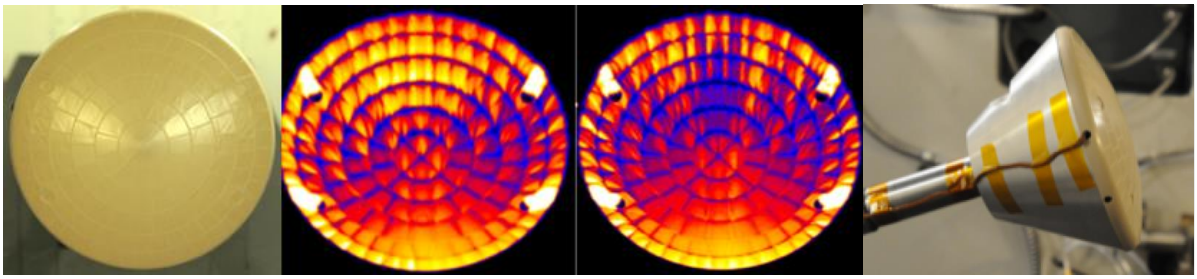

Fig. 7 IR thermography data on PEEK Orion forebody model tested in the 20-Inch Mach 6 Air Tunnel [Photos Source: NASA].

B. Artemis I Post-Flight Analyses

The Artemis I mission was flown in 2022 to demonstrate the performance of the Orion MPCV heat shield, which differed from the heat shield configuration for the EFT-1 mission. Post-flight evaluation of the heat shield revealed it experienced unexpected char-loss at multiple locations on the heat shield. Thus, an extensive test program was

conducted in the LaRC 20-Inch Mach 6 Air Tunnel to obtain aeroheating data on a wide range of possible char-loss cavity sizes and locations. Sample global phosphor thermography aeroheating images of the pre-flight capsule (without char-loss cavities) are shown in Fig. 8 for a range of Reynolds numbers. Heating augmentation can be seen around the four attachment-point cavities for all cases and boundary-layer transition can be observed on the leeside of the vehicle (top of image) for the highest Reynolds number case.

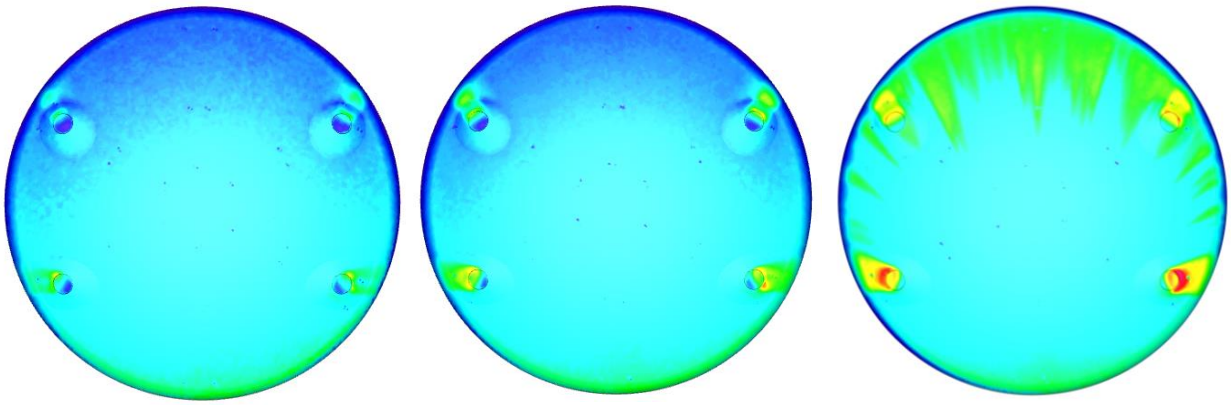

Low Reynolds number Moderate Reynolds number High Reynolds number

Fig. 8 Aeroheating data on the Orion heat shield.

C. Low-earth Orbit Flight Test of an Inflatable Decelerator (LOFTID)

The LOFTID project successfully demonstrated the performance of a Hypersonic Inflatable Aerodynamic Decelerator (HIAD) at operational mission relevant conditions in November 2022 [28]. The LOFTID vehicle (Fig. 9) is comprised of a rigid centerbody/payload module that contains the inflatable aeroshell. Upon deployment, the seven supporting toroids inflate, and the flexible thermal protection system (F-TPS) covering the toroids forms a 70° sphere-cone geometry. The F-TPS protects the front of the aeroshell during reentry; however, the back face of the aeroshell has no thermal protection, fully exposing the toroids to the wake flow.

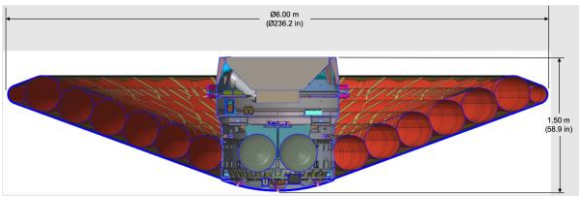

Vehicle cross section

Infrared image of aeroshell after splashdown (Photo Source: NASA)

Fig. 9 LOFTID vehicle CAD geometry and flight vehicle images.

The LAL facilities supported this mission through testing to obtain aeroheating and boundary-layer transition data for development of the vehicle's flight database. The test campaign was focused on two elements of the flight environment that are not amenable to computational simulations: 1) the influence of deflections in the outer mold line of the F-TPS on boundary-layer transition and convective heating and 2) the heating levels in the separated, unsteady wake flow over the back-face of the aeroshell.

1. Flexible thermal protection system scalloping effects on aeroshell heating

The OML of a HIAD F-TPS will deform under aerodynamic pressure loading. The patterns formed by the deflection of the F-TPS over the structural toroids and the tension tie straps that hold them together is referred to as

scalloping. This scalloping may potentially promote earlier boundary-layer transition onset compared to a rigid aeroshell and produce turbulent heating augmentation above smooth-surface levels. For the LOFTID wind tunnel test campaign, wind tunnel models with different scallop depths were tested in the 20-Inch Mach 6 Air Tunnel over a Reynolds number range sufficient to produce laminar, transitional, and turbulent flow (Fig. 10). Global phosphor thermography was used to obtain surface heating distributions. Although the complete set of test data demonstrated the potential for high turbulent heating augmentation over large scallop depths at high Reynolds numbers, the data relevant to LOFTID's flight conditions showed that the scallop heating augmentation effects were minimal and fell within the performance limits of the vehicle's F-TPS.

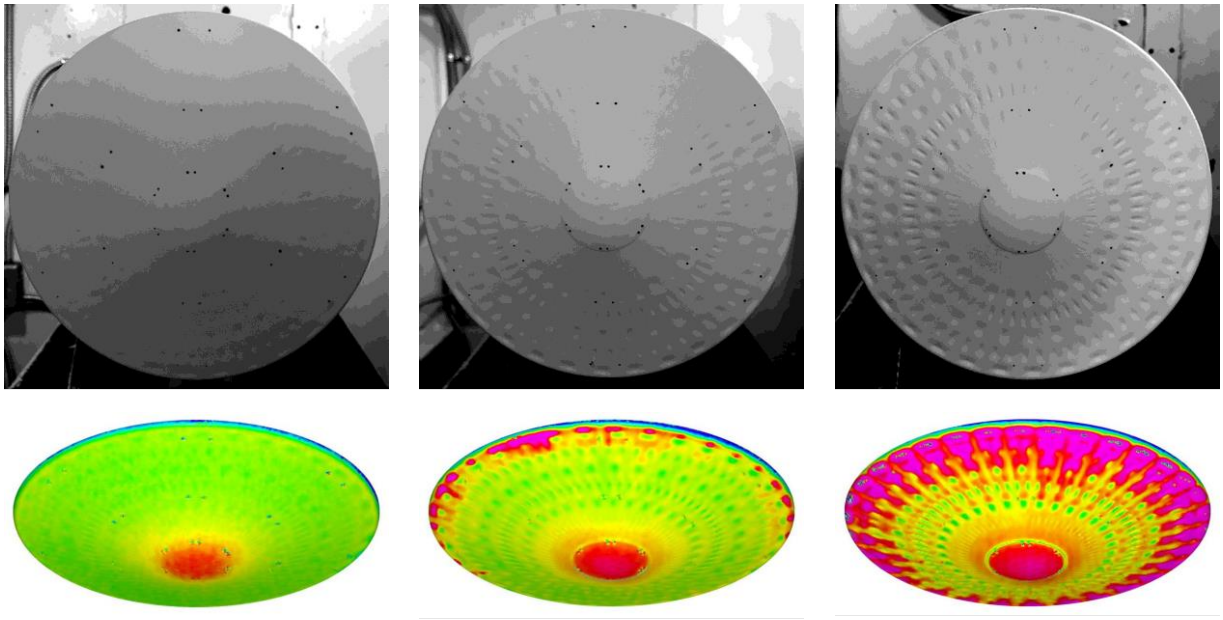

Minimum scalloping | Nominal scalloping | Maximum scalloping

Fig. 10 LOFTID aeroshell scalloping ceramic models and heating contour maps [Photos Source: NASA].

2. Aeroshell back-face and payload heating

Prediction of the LOFTID vehicle's wake flow structure, and the resulting aeroshell back-face and payload surface heating, proved to be an extremely challenging computational task due to the unsteady, three-dimensional (3-D) transitional/turbulent character of the flow and the complex topology created by the concave backshell and exposed structural toroids. Although computational methods were employed to predict the flight vehicle environments, these predictions were assigned high (± 100%) uncertainty levels. An intensive and ongoing test campaign to obtain surface aeroheating (Fig. 11) and wake flowfield visualization data to validate the computations was sponsored jointly by the LOFTID program and the NASA Entry Systems Modeling project. Back-face heating data obtained via global phosphor thermography (Fig. 12) demonstrated that the computational methods provided accurate results, and testing continues to obtain more validation data to provide a better definition of the computational uncertainty margins.

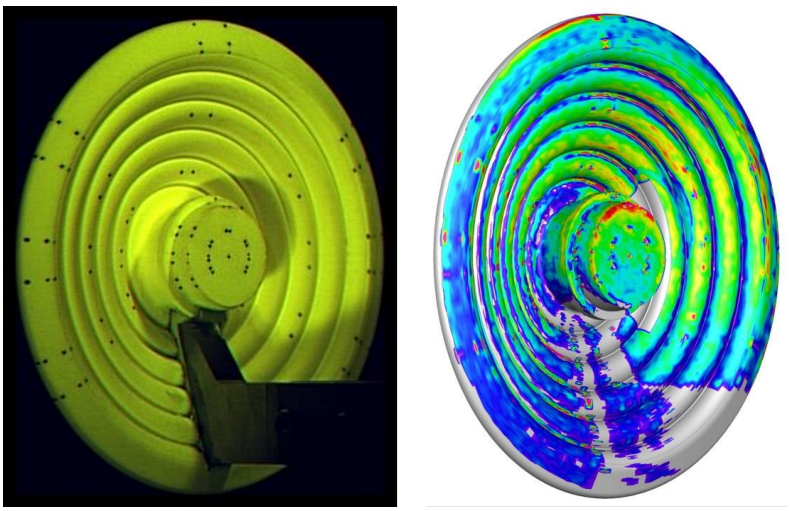

Raw intensity image Processed heating data

Fig. 11 LOFTID aer and him him him oshell back-face heating data.

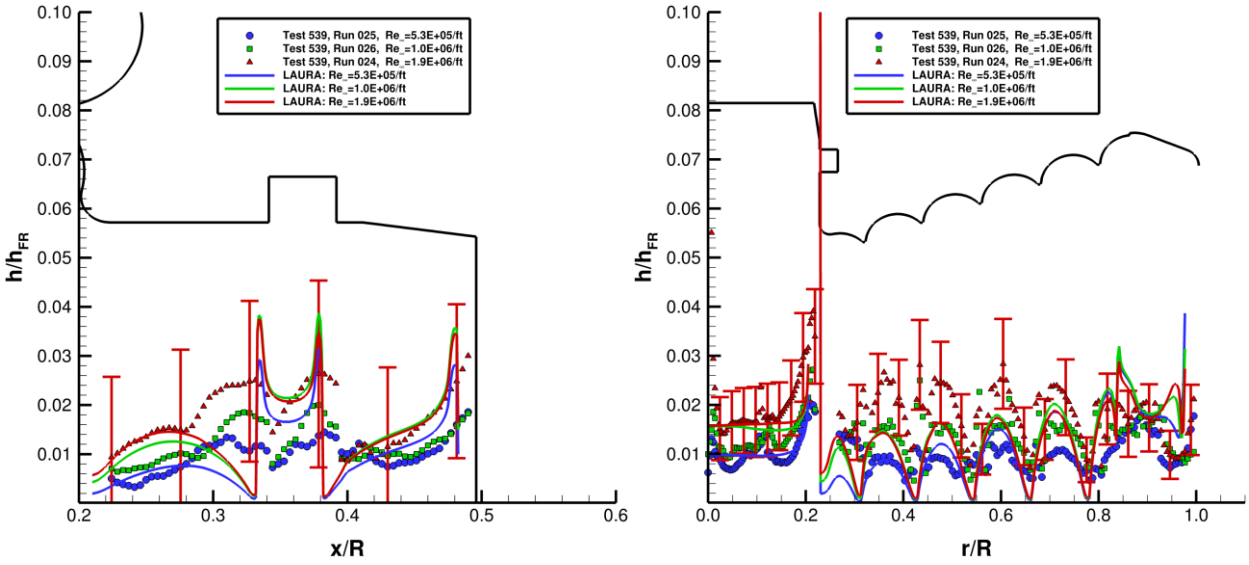

LOFTID center body/payload LOFTID aeroshell back face

Fig. 12 Comparison of predicted and measured LOFTID heating.

D. Boundary Layer Transition (BOLT) Flight Project

NASA LaRC has been actively supporting the Air Force Research Laboratory (AFRL) and Air Force Office of Scientific Research (AFOSR) BOLT flight project. The goal of BOLT, an acronym for Boundary-Layer Transition or Turbulence, is to study the boundary layer on a representative hypersonic vehicle using sounding rockets to obtain flight conditions near Mach 6. The boundary layer (BL) is an important consideration for hypersonic vehicles, as surface temperatures are strongly dependent on BL state (laminar vs. turbulent), with convective heating rates many times higher when turbulent. There have been two flight attempts to date, with plans for a third. The two flights include BOLT-1, launched out of Esrange, Sweden in May of 2021, and BOLT-2, which flew out of NASA Wallops Flight Facility (WFF) in Virginia during March of 2022. The focus of BOLT-1 was to obtain detailed measurements

of the boundary-layer transition process; however, due to a staging issue, the research vehicle did not reach planned flight conditions (see Ref. 30). There are plans underway to redo this flight in the future, which will be called BOLT-1B. The BOLT-2 flight was more focused on obtaining high quality flight data of the turbulence downstream of transition onset, so the geometry was elongated as a result. This flight was fully successful, and preliminary data and analysis have been published, e.g., see Refs. 31 and 32.

A series of BOLT wind tunnel studies have been conducted at NASA LaRC, specifically in the 20-Inch Mach 6 Air Tunnel, supported by the Hypersonic Technology Project (HTP). Table 1 provides a list of the recent BOLT specific test entries conducted within that facility, identifying the configuration, the model scale, and the test techniques utilized. The initial set of wind tunnel data presented at the project kickoff meeting in 2017 was obtained during Test 7027, conducted within one month of delivery of the geometry CAD file, and published in Ref. 33. That model was a half-scale version of the original BOLT geometry, whose full-scale length was 34.1-in, and the test technique utilized LaRC's phosphor thermography system. There have been several subsequent wind tunnel entries into the same facility to study various aerothermal issues, such as surface roughness, including step effects, distributed leading edge roughness, and isolated trips, and heating to fairings connecting the flight vehicle to the launch stack [34]. Note that between the BOLT-1 and BOLT-2 flights, there was an attempt to increase the running length of the flight vehicle, with the introduction of the Long-BOLT configuration that was almost twice as long as BOLT-1. In the end, BOLT-2 only ended up being about 15% longer due to concerns regarding the controllability of the launch vehicle stack. Figure 13 provides a sketch representing full-scale versions under consideration, indicating the locations of various surface features, such as the nose joints and the trip locations. Many of the BOLT-2 specific studies were conducted on a Long-BOLT model since the shorter BOLT-2 length was well captured.

Table 1. List of BOLT related studies in the LaRC 20-Inch Mach 6 Air Tunnel.

Test #	Configuration - Technique	Model Scale	Model Length	Model Nose Radius
7027	BOLT - Phosphor	Half	17”	0.0985”
7031 & 7077	BOLT LE Roughness - IR	Third	11.4”	0.066”
7032	BOLT Roughness – IR, Pressure	Third	11.4”	0.066”
7041	BOLT Fairing - Phosphor	Quarter	8.52” (BOLT section)	0.049”
7056	Long-BOLT - Phosphor	30%	17.7”	0.0591”
7067 & 7071	Long-BOLT - IR	Half	29.5”	0.0985”
7092	Long-BOLT – IR ZOOM	Half	29.5”	0.0985”

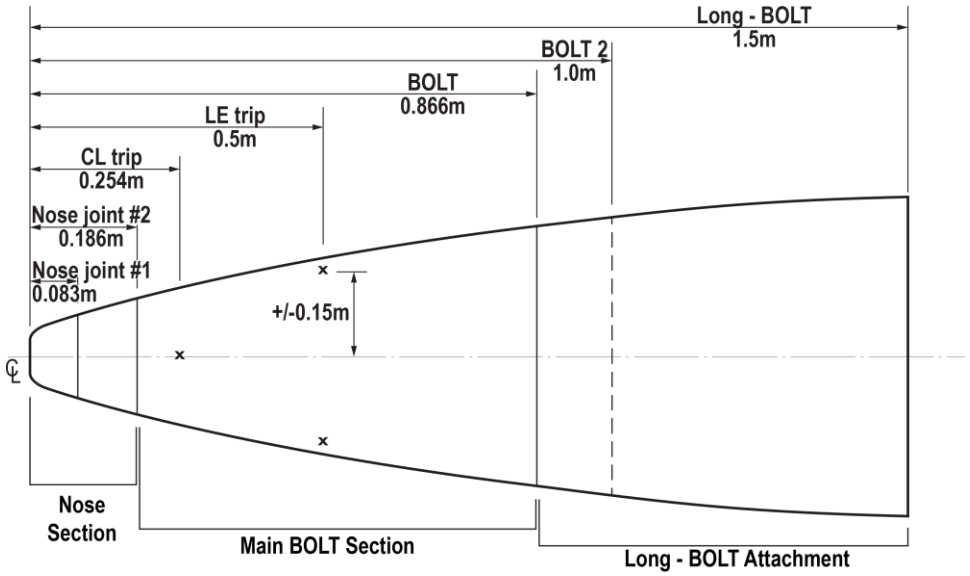

Fig. 13 Full-scale dimensions of various BOLT configurations considered by the project.

For the initial BOLT study, the quick fabrication capability inherent to the phosphor thermography technique benefitted the project. With follow on studies, there was a desire to compare test techniques by utilizing a relatively new IR thermography approach with machined PEEK substrates as the model material. One advantage of building models with this slower approach is that very small surface features could be more accurately replicated using precision machining or laser-ablation methods. Thus, in the follow-on study of Test 7031, and then later with Test 7077, PEEK models were built that included various small regions of distributed surface roughness, including both random and periodic types, along the leading edges and near the nose. Figure 14 provides a side-by-side comparison of representative images from those two test entries, showing that with two different test techniques and model scales, the results are similar for comparable length Reynolds numbers. Additional results from these wind tunnel entries were captured in Ref. 31, along with comparisons to CFD simulation results.

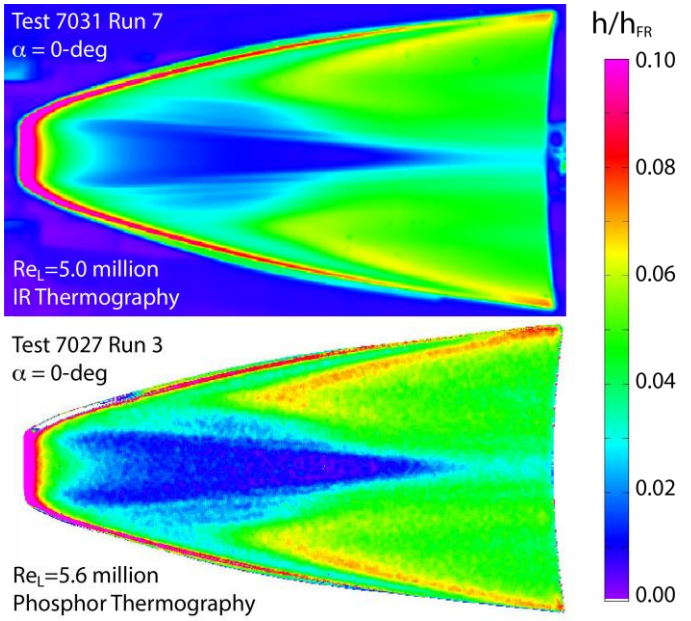

Fig. 14 Comparison of test techniques and model scales supporting BOLT-1.

After a successful demonstration of the experimental approach using PEEK models with IR thermography, additional studies were initiated to allow improved precision of small features of interest, such as the impact of tiny joint steps (either forward or rear facing) at the nose joint and discrete and distributed roughness. A half-scale Long-BOLT model was designed and fabricated to permit parametric variation of the joint step, at the second nose joint shown in Fig. 13, in very small increments (±0.001") and the placement of discrete trips at locations corresponding to the flight of BOLT-2. Preliminary results of the wind tunnel tripping study were recently published in Refs. 35 and 36. The parametric step study was recently completed, and the analyzed results will be shared in an upcoming paper (at AIAA Aviation 2024). Figure 15 provides a comparison of representative images from a phosphor and IR study to investigate step effects and tripping, again showing similar results. The IR data is considered preliminary due to changes to the pretest calibration, so the color scale differs for the two images.

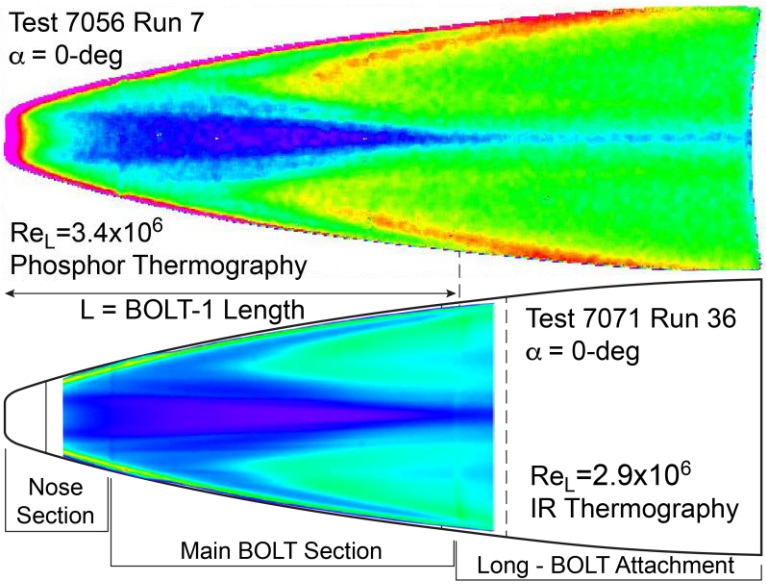

Fig. 15 Comparison of test techniques and model scales supporting BOLT-2.

E. Mars Sample Return Earth Entry System

The NASA Mars Sample Return (MSR) Earth Entry Systems (EES) flight mission aeroshell will employ a 3-D Mid Density Carbon Phenolic (3MDCP) heatshield material. This woven TPS material results in a patterned rough surface after charring, with the pattern following the weave topology. This patterned roughness results in early boundary-layer transition and turbulent convective heating augmentation. Furthermore, the cone angle of the EES forebody is 52.5 degrees, which results in supersonic flow remaining deep into the boundary layer near the roughness elements. There were no existing aeroheating measurements of the roughness augmentation of a patterned roughness surface with supersonic flow near the roughness elements prior to this study. This motivated the EES test campaign in the Langley Mach 6 facility to obtain such measurements. Leveraging recent patterned roughness measurements in this facility, a range of patterned roughness models were constructed for a 52.5° sphere cone, which represents the EES geometry. Figure 16 illustrates the heating augmentation in the turbulent region downstream of the trip ring on the smooth OML section, which was compared to baseline heating in the laminar smooth region and turbulent heating levels on the rough sections of the model. The sphere-cone models represent the EES geometry, while the flat plate models enable supersonic flow deeper into the boundary layer at the Mach 6 test condition. The flat plate models also enable heating measurements to the bottom of cavities built into the plate, which are used to validate micrometeoroid

damage simulations relevant to EES. The heating measurements obtained on these models will be used to tune EES roughness augmentation models and inform the convective heating margin.

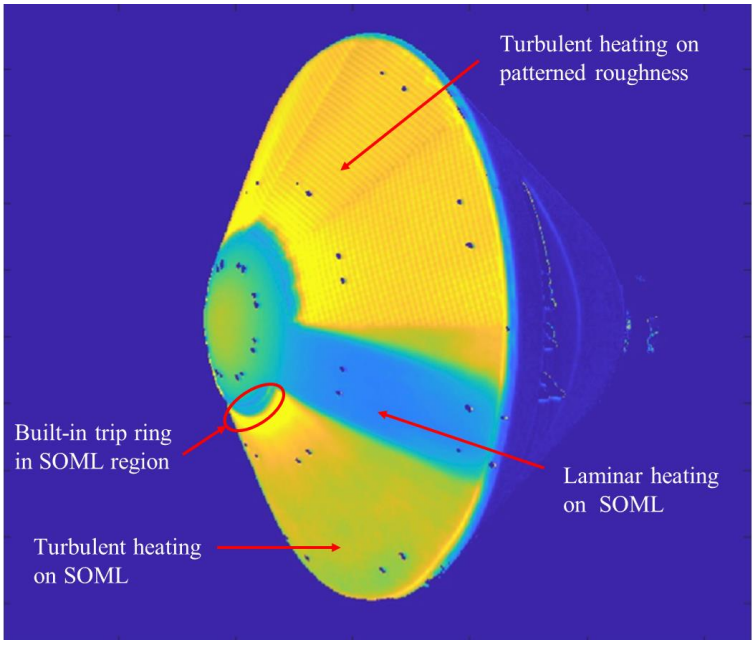

Fig. 16 Example of an MSR-EES surface heating contour map for a Re = 5x10^6/ft case [37].

IV. Research and Development

In addition to direct support for the development of NASA flight programs, the Langley experimental aerothermodynamics capabilities are also employed in the development of entry, descent, and landing (EDL) technologies, CFD validation, and entry vehicle preliminary design studies and configuration assessment. Highlights of recent research and development programs are presented in this section, some of which are ongoing efforts that have not yet been published elsewhere.

A. Arnold Engineering Development Complex (AEDC) Tunnel 9 Cone Boundary-Layer Transition Model

A stainless steel, instrumented, 7º half-angle cone developed for testing in the Arnold Engineering Development Complex (AEDC) Tunnel 9 was brought to NASA LaRC for boundary-layer transition studies in the LAL wind tunnels. The effects of off-nominal wind tunnel flow conditions, nose-tip radius, and shaped roughness elements on instability growth and boundary-layer transition were investigated.

1. Nose-tip Bluntness

The dominant instability mechanism that triggers boundary-layer transition on sharp cones at 0º incidence is the second-mode instability. The mechanism for blunt-nose transition on a cone is not well understood. Roughness-induced transient growth is speculated to be the cause [38]. Both conventional LAL facilities were utilized with a bevy of diagnostics to measure the instability growth and transition behavior on the cone. The model was instrumented with surface-mounted Kulite and PCB pressure transducers and thermocouples. Off-body measurements included high-speed schlieren [39] and focused laser differential interferometry (FLDI) [40]. Data were acquired for ten nose-tip radii, ranging from 0.006 to 0.5 in. While second-mode disturbances were evident for the sharper noses, as expected, these modal disturbances became progressively weaker with increasing radius and were not observed on the cones with blunter noses. The surface and off-body optical measurements will be used to improve the understanding of BLT on blunt cones and to develop improved physics-based transition prediction models for these configurations.

2. Supercooled Flow

The AEDC Tunnel 9 cone model was tested with the sharp nose tip in the 31-Inch Mach 10 Air Tunnel at off-nominal, supercooled tunnel flow conditions [41]. Lowering the total temperature weakened the second-mode instability that typically induces boundary-layer transition on a cone, despite the increase in Reynolds number compared to the standard flow conditions. In addition to the surface pressure and temperature measurements, the freestream stagnation pressure was measured using a pitot probe. The correlation between the level of supercooling, the measured total pressure, and the pressure fluctuations on the model surface will inform computational models on the effect of supercooling on the growth of second mode instabilities. These supercooled measurements may also impact future hypersonic wind tunnel designs as they provide lower limits for a total temperature impacting freestream total pressure and cone static pressure.

3. Roughness elements

A 20-Inch Mach 6 Air Tunnel entry investigated the effect of adding shaped roughness arrays to the surface of the AEDC cone on the second-mode instability and the transition location [42]. Elliptic-planform elements of six different heights and two other elements shapes of moderate height were tested. A single vortex-generator (VG) array was adhered to the cone for each run with the elements centered 9 in. downstream of the sharp nose tip. Figure 17 shows the location of the VG array on the cone and the relative positions of the pressure transducers, static pressure ports, and thermocouples. The acquired pressure fluctuations and temperatures downstream of the array suggested the taller roughness elements strongly reduced the second-mode instability, but also increased the lower-frequency content. Thus, reducing the second-mode instability did not generally result in a measurable delay in transition. This study improves the understanding of the effect of roughness on transition and will facilitate improved physics-based transition prediction models.

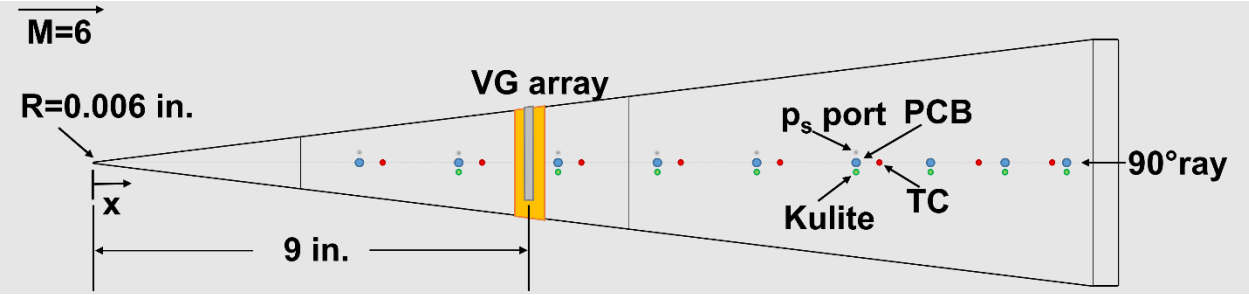

Fig. 17 Diagram of AEDC Tunnel 9 stainless steel, instrumented, 7º half-angle cone.

B. Entry Systems Modeling Project – Mission Relevant Roughness

The NASA Entry Systems Modeling project has sponsored a series of wind tunnel tests [43-45] to obtain data on boundary-layer transition and turbulent heating augmentation due to roughness. Several forms of "mission-relevant" roughness (Fig. 18) were considered which have direct traceability to past or future NASA missions, including ablated hexcomb patterns (Apollo missions and Orion EFT-1), sand-grain roughness (Stardust and Genesis), block-TPS steps and gaps (MSL, Mars 2020, Artemis I) and woven TPS (Mars Sample Return – Earth Entry System).

All testing was conducted in the 20-Inch Mach 6 Air Tunnel and data were obtained using global phosphor thermography. Two model geometries were considered – a spherical-cap like the Orion capsule and a sphere-cone similar to the MSL entry vehicle. Multiple models of each configuration were fabricated with a variety of roughness heights and were tested over a range of Reynolds numbers sufficient to produce laminar, transition and turbulent flows.

TPS roughness was found to promote boundary-layer transition well before "smooth-wall" onset and turbulent heating augmentation was measured at levels well-above "smooth-wall" turbulent data and/or predictions (Fig. 19). These data sets are intended to be used both in the development and validation of numerical models for simulation of

roughness-dominated flows and to directly support the development of aeroheating environment databases for future missions.

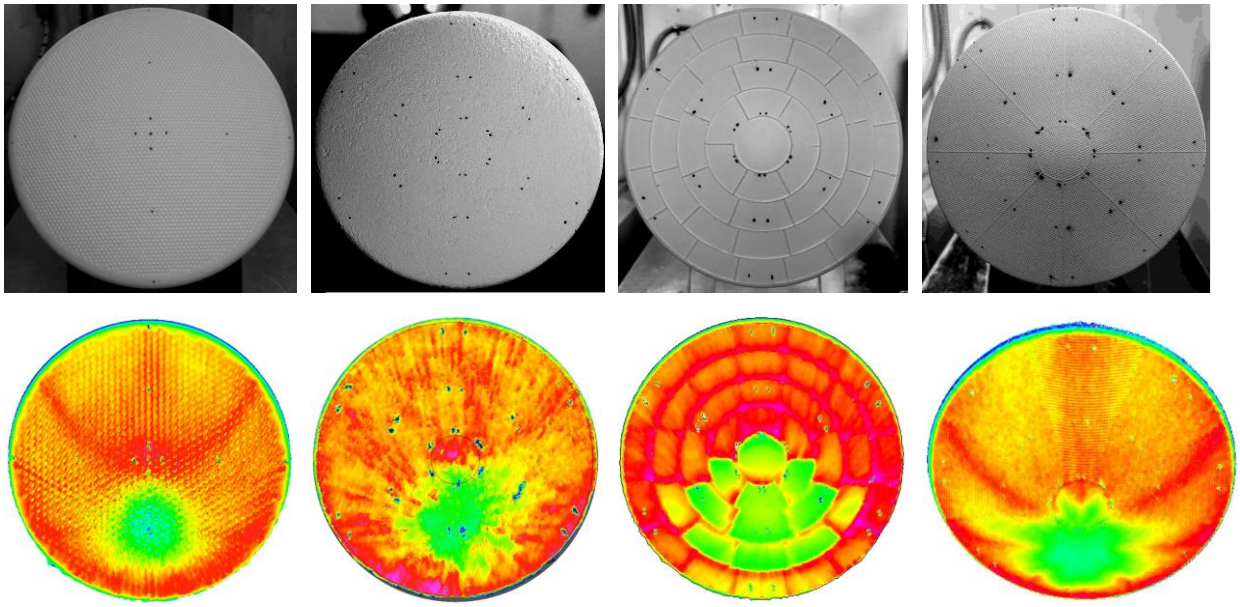

Hexcomb roughness | Sand-grain roughness | Step/Gap roughness | Woven roughness

Fig. 18 Mission relevant roughness models and sample aeroheating data [Photos Source: NASA].

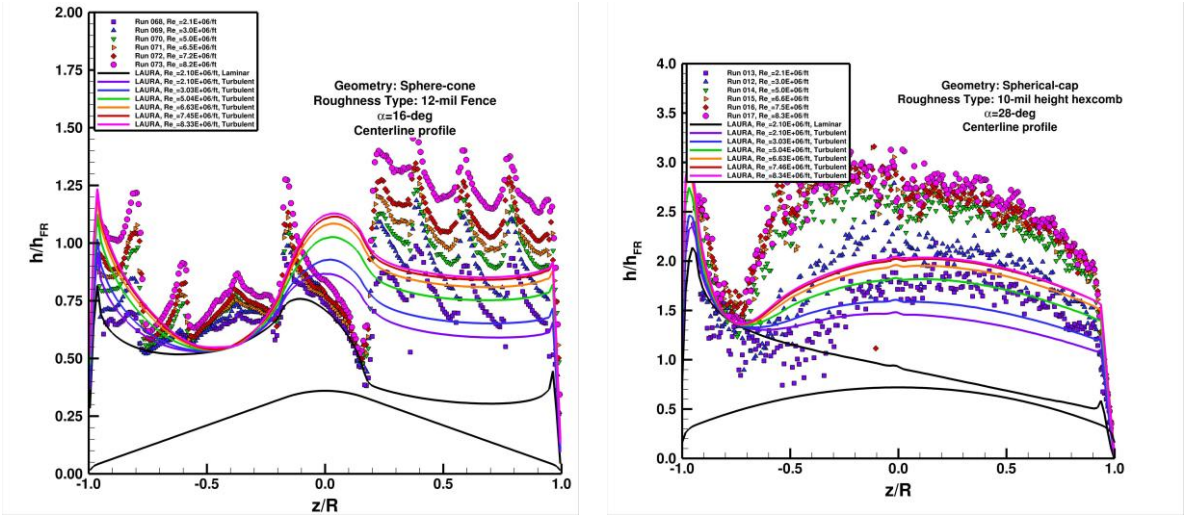

Hexcomb roughness on sphere-cone geometry | Block-TPS fences on spherical-cap geometry

Fig. 19 Transition and heating augmentation effects due to roughness.

C. Cone-Slice-Flap – Aerodynamic Design of Experiments

Akin to the transonic NASA common research model (CRM) and the supersonic AGARD-B configuration, members of the NASA Aerosciences Evaluation and Test Capabilities (AETC) Wind Tunnel Characterization Working Group proposed a general research configuration of a blunted, slender cone that includes a body slice and flap as a common check standard model for hypersonic wind tunnel testing. Design of Experiment (DoE) principles were applied to a parametric database of preliminary computational simulations and the experimental wind tunnel matrix to select 33 CSF configurations varying the nose radius, slice length, flap location and flap deflection to test over a range of angle of attack and Re number conditions. The 7° half-angle, blunted cone/slice/flap (CSF) geometry recently tested in the NASA LAL shares configuration parameters with the CSF designs previously tested by Oberkampf, Sandia National Laboratories and Purdue University [46, 47]. A blunt nose offers two advantages over a sharp (R_N = 0) nose: 1) a 0.023-inch-diameter orifice fits in the sharpest nose tip (nose radius/base radius, R_N/R_B, = 0.04) in the design space without adversely affecting the local flow near the stagnation point, and 2) a blunt nose tip is less fragile and less likely to change diameter than a theoretically sharp nose. The aerodynamic experimental results from the LAL DoE study demonstrate the CFD model-form uncertainty estimate can account for 86% of the total uncertainty in model predictions. Aerodynamic characteristics acquired in the parametric study will be used to validate multiple CFD models.

Additional computational simulations were conducted to pinpoint the model geometric features most likely to affect CSF aeroheating profiles. An aerothermal test was conducted in the 20-Inch Mach 6 Air Tunnel using cast ceramic models with varying nose bluntness and flap deflection angles to acquire experimental heating and boundary-layer transition data. The primary six models considered in this study are shown in Fig. 20, with changing R_N/R_B ratios and flap deflection angle (θ_f). Aeroheating data were collected on the LaRC aerodynamic check standard model configuration, model 5, using a run matrix defined by Design of Experiments principles. Additional data were collected on cone-slice-flap geometries with different slice and flap definitions like models previously tested under both "noisy" and "quiet" flow conditions at Purdue University (not shown in the figure) with blunter nose tips. These experimental results will support uncertainty quantification in academic collaborations with the Missouri University of Science and Technology, a University Consortium for Applied Hypersonics (UCAH) partner, and will be used to validate the NASA CFD simulations designed to predict the aeroheating behavior.

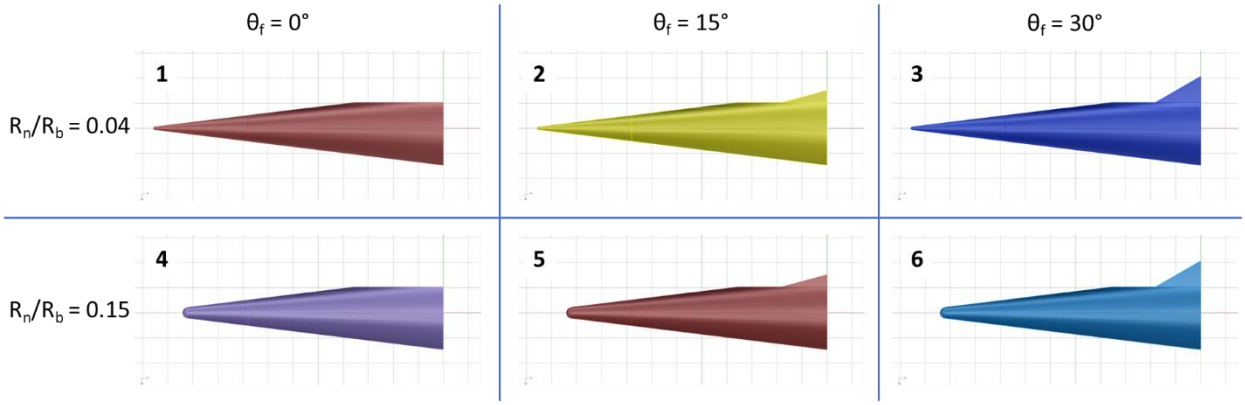

Fig. 20 Primary CSF geometries tested in the 20-Inch Mach 6 Air Tunnel aeroheating study.

D. Dynamic Balance Demonstration

The measurement of transient events is of interest to many groups, for scenarios such as control thruster firings, shroud separation, and rapid control surface deflection. A cooperative effort [46] between the NASA Langley Research Center and the Johns Hopkins University Applied Physics Lab (JHU/APL) successfully used a rapidly-actuated-flap cone model to provide near-impulse loads that were measured by a piezoelectric-transducer force measurement system, simultaneously with a conventional strain-gage balance. The test was conducted in the NASA

Langley 31-Inch Mach 10 Air Tunnel using a 7° sliced-cone model fabricated of titanium. A remotely controlled servo was used to drive the flap, which was capable of deflections up to 35°. Typically, the movement from 0° to 30° deflection was accomplished in less than 40 milliseconds. Variations in flap deflection, angle of attack, and Reynolds number were used to impart loads of different magnitudes. A high-speed camera was used to verify flap deflection with time. A diagram and image of the rapidly-actuated-flap cone model is shown in Fig. 21.

A comparison of the piezoelectric-transducer and conventional-balance data will show the benefits and limitations of each method. The data also will be used to validate various data reduction techniques. This work will provide a capability to measure the aerodynamic effects of transient events, such as the rapid movement of control surfaces, as well as a simultaneous measurement of steady-state loads, in a high-speed environment. Eventual applications include a study of the aeroelastic effects of the control surface on a hypersonic vehicle.

The data plot in Fig. 22 shows the conventional strain-gage balance data acquired in the dynamic balance study. The dark blue line shows the balance data recorded at 25kHz, while the light blue line represents data acquired at 100 Hz from the standard LAL facility force data acquisition and reduction. Red lines indicate either start of flap movement (vertical line) or mean load levels (horizontal lines).

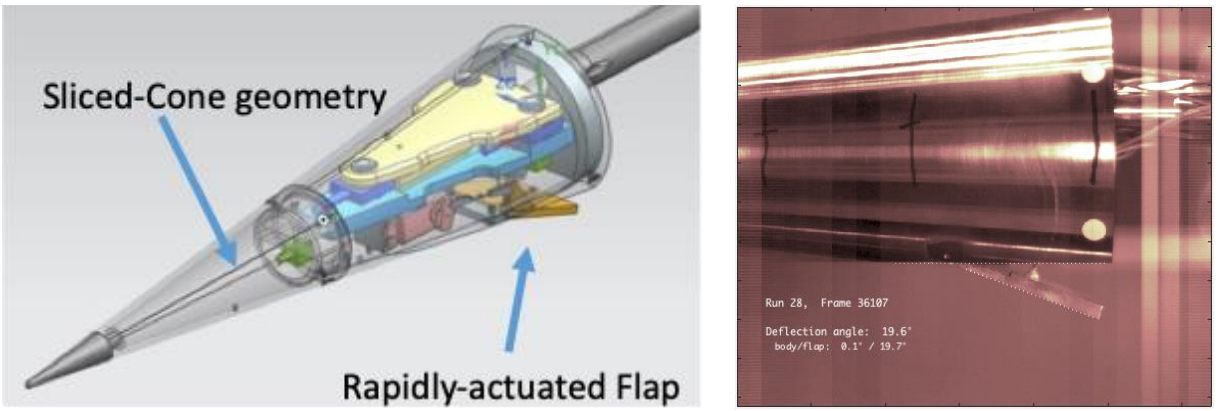

Fig. 21 Diagram and photograph of cone model with actuated flap [Photo Source: NASA].

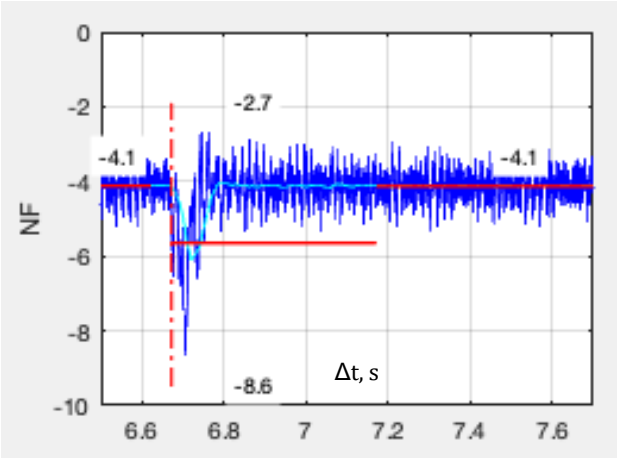

Fig. 22 Normal force vs. time during actuation of the flap.

E. Aerodynamic Trim Tabs on Decelerator Aeroshells

Numerous NASA and external flight programs are investigating hypersonic aerodynamic decelerators to safely carry payloads through the EDL phase of entry to earth or Mars. Adding trim tabs to the aeroshell can provide beneficial moment control in either pitch or yaw and establish a non-zero trim angle of attack for HIAD and rigid decelerator configurations. Aerodynamic coefficients were obtained over an angle-of-attack range from -4° to 28° for models with up to four trim tabs, at a Mach number of 6 and two Reynolds numbers, with either 0° or non-zero sideslip angles. Schlieren and IR thermography data (shown in Figs. 23 and 24) also were measured on these blunt body models to qualitatively visualize the effects of boundary-layer trips and wake impingement. Several models were manufactured using a rapid-prototyping process and assessed for future use in aerodynamic studies (e.g., Fig. 23b). The use of trim tabs extends the trim range significantly. Only minimal coupling between pitch and yaw planes was observed that might affect global navigation and control of the decelerators. This test complemented an earlier test [49, 50] in the Langley Unitary Plan Wind Tunnel (LUPWT), extending the Mach number range of the dataset from 4.6 to 6, and adding additional trim tab configurations.

a) b) c)

Fig. 23 a) Metallic trim tab models [Photo Source: NASA], b) prototyped models, c) surface IR thermography contour map.

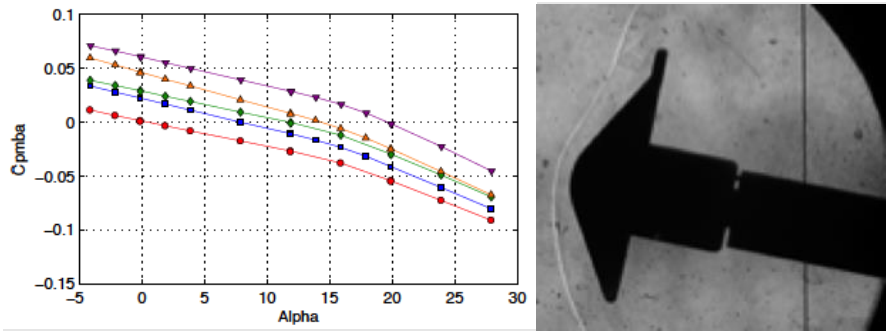

a) b)

Fig. 24 a) Variation in model coefficients with alpha and b) schlieren photograph of a trim tab model.

V. Commercial and Defense Partnerships

The LAL facilities are frequently used for programs where testing is performed by NASA personnel in support of commercial and defense partners. However, data restrictions prohibit sharing of results from these tests. Procedures are in place in the LAL for the conduct of Proprietary, Controlled Unclassified Information (CUI), International Traffic in Arms Regulation (ITAR), and Classified testing programs.

VI. Academic Partnerships

Universities collaborate with NASA Langley Researchers to conduct studies in the areas of fundamental aerodynamic research and testing such as boundary-layer transition, shock-wave/boundary-layer interactions, and fluid-thermal-structural interactions.

A. Purdue University: Cone-Fin Study

Hypersonic flight vehicles often have fin-body and wing-body junctions with complex viscous-inviscid interactions in which boundary-layer transition is not well understood. It is critical to understand the impact of the boundary-layer state on heating and separation in these flows and to be able to predict the transition location. Tools for transition prediction are rapidly improving, but still cannot be relied upon for an arbitrary geometry necessitating the need for ground tests to inform computational models. To aid the development of prediction methodologies for complex 3-D geometries, measurements of instability and transition were obtained for a highly swept fin mounted to a slender cone in the 20-Inch Mach 6 Air Tunnel over a range of freestream Reynolds numbers [51]. The transition location was inferred from the surface heat flux distribution, derived from IR thermography, and compared to complementary measurements obtained in the Boeing/AFOSR Mach-6 Quiet Tunnel at Purdue University (Fig. 25). It was demonstrated that freestream noise generated by the turbulent boundary layers along the wind tunnel nozzle walls in the conventional LAL facility caused transition at length Reynolds numbers nearly 50% lower than was observed in the quiet facility (Fig. 26). Corresponding surface pressure fluctuation measurements demonstrated that freestream noise also changed the dominant instability mechanism leading to transition.

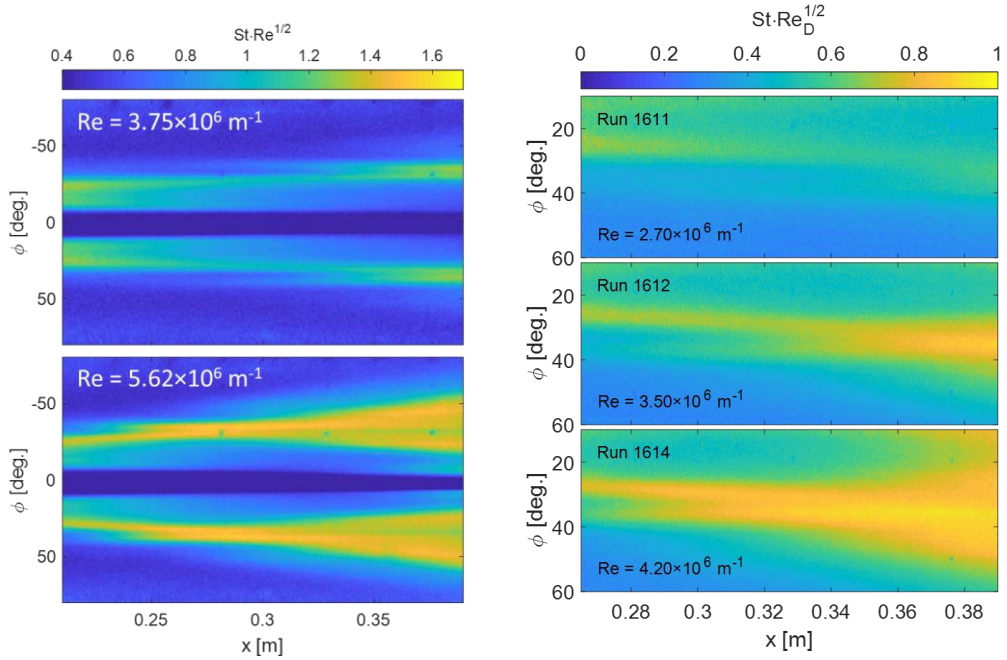

a) b)

Fig. 25 a) LAL 20M6, p'/prms ≈ 1.5% b) BAM6QT noisy, p'/prms ≈ 3%

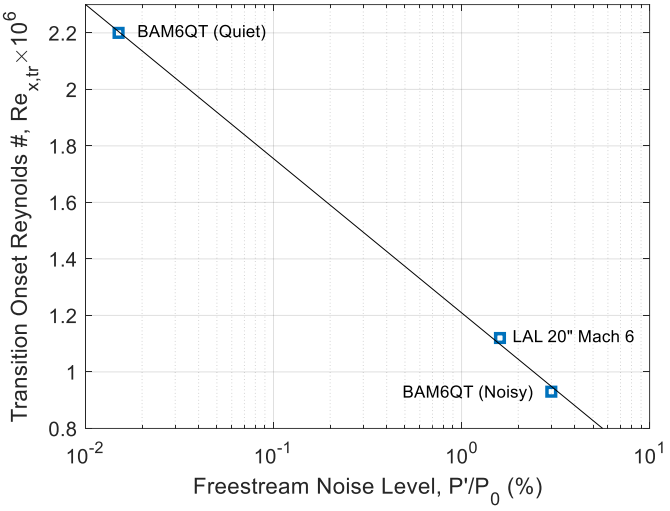

Fig. 26 Transition onset Reynolds number scales with the freestream noise.

B. University of Maryland: Flat Plate with Compliant Panels Ramp

Fluid-thermal-structural interactions (FTSI) present challenges for hypersonic flight vehicles where thin skins, surface panels, and control fins are designed to minimize weight. A collaboration with University of Maryland has been in place since 2017 to test FTSI in LAL hypersonic facilities. Results of the most recent experiment were presented by Schöneich [52], where FTSI of a compliant panel embedded in a compression ramp at Mach 6 are explored. The panel structural response is investigated for turbulent and transitional shock-wave/boundary-layer interactions (SWBLI). Fast-response piezoresistive pressure transducers positioned upstream of the compression corner and simultaneous full-field photogrammetry and IR thermography are used to measure panel deformation and temperature.

A plenum box behind the compliant panel is used to control the static pressure differential across the panel. A CAD rendering of the test model is shown in Fig. 27. The ramp has interchangeable mounting brackets for ramp angles of 10°, 20°, 30°, 34°, and 38°, spanning flow conditions from attached to fully separated. An example of IR thermography temperature data on the panel centerline are presented in Fig. 28. These results show greater heating near the leading edge of the panel. As the static pressure differential increases, the panel displacement equilibrium and temperature distribution shift. An earlier investigation, Whalen et al. [53], theorized that heating the panel strongly affected the changes in the natural frequencies of the panel modes. These experiments, Schöneich et al. [54], confirmed that the thermal effects on the model directly led to the frequency shift in the natural vibrations of the panel. Figure 29 shows a comparison of two methods for interpreting the frequencies associated with structural vibratory modes, which are correlated with the panel temperatures during a run. Figure 29 a) uses a spectral proper orthogonal decomposition (SPOD) method to interpret the photogrammetry data from high-speed cameras (31 kHz). SPOD uses data from all the markers to determine the dynamic modes at each frequency and characterizes the overall panel motion rather than at discrete points. Figure 29 b) interprets the fast-response piezoresistive pressure transducer data in the plenum box using Welch's block method. By using a pressure transducer, the frequency shift across the entire run time can be traced rather than only the interrogation time of the photogrammetry cameras.

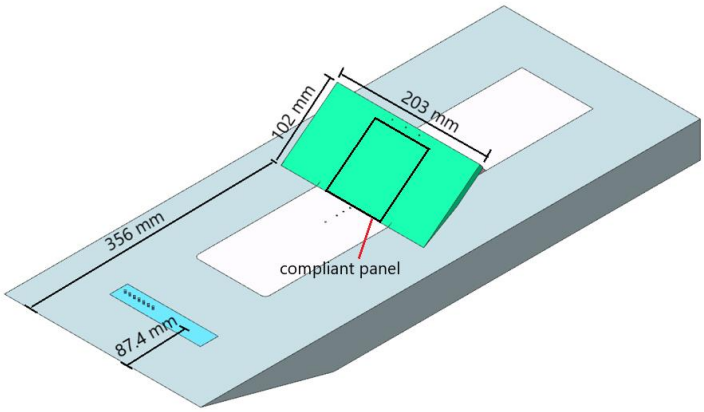

Fig. 27 CAD rendering of the model with trips.

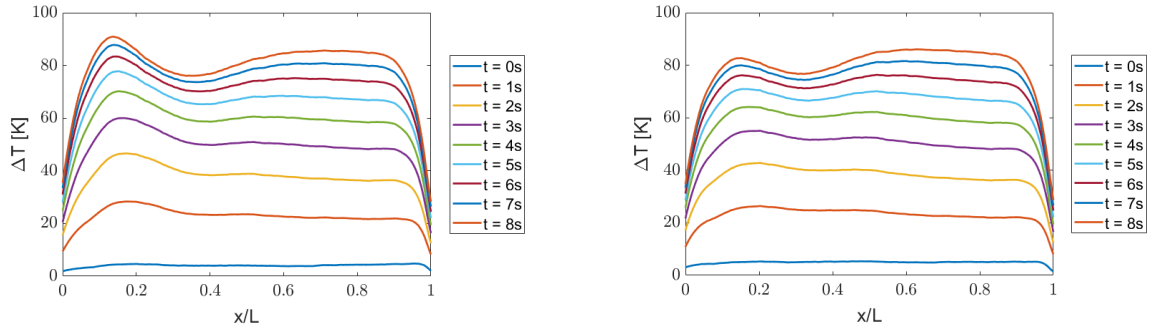

a) b)

Fig. 28 Span-averaged temperature difference between the compliant panel and the ramp support at 34°, Re=2.0 x 10^6 ft^{-1}, no trip strip, with pressure differentials of a) 0 kPa and b) 1.93 kPa.

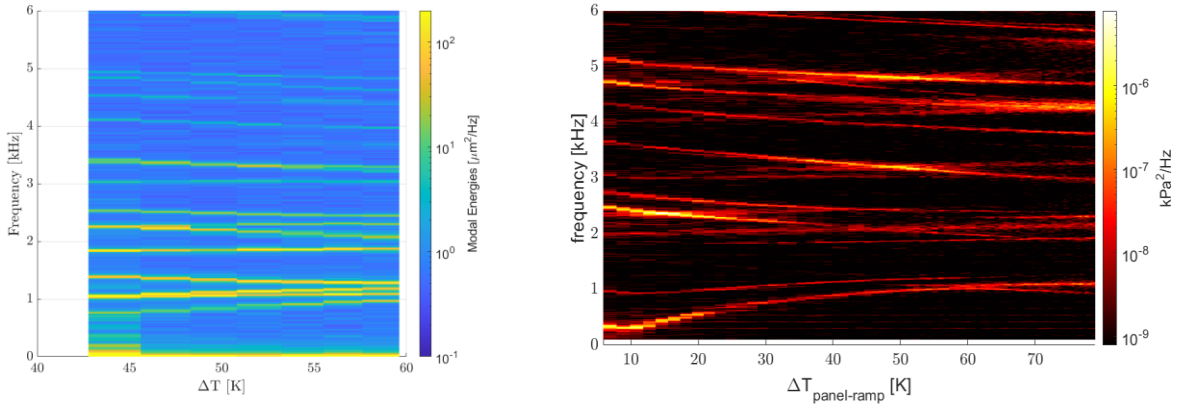

a) b)

Fig. 29 Panel modal frequencies correlated to the change in temperature using a) SPOD of the out-of-plane displacement and b) Welch's method on the static pressure signal inside the plenum box.

C. University of Tennessee Space Institute, University of Texas at San Antonio: Shock-Wave/Boundary-Layer Interactions

In collaboration with the University of Tennessee Space Institute and University of Texas at San Antonio, NASA tested both a wedge and a flat plate model with and without a cylinder or ramp shock-generating elements in the LAL 20-Inch Mach 6 and the 31-Inch Mach 10 Air Tunnels, respectively, across a range of Reynolds numbers [55]. The purpose of this study was to observe the resulting shock-wave/boundary-layer interactions (SWBLI) upstream of the cylinder or ramp mounted to the top surface of the model. The interaction upstream of a cylindrical protuberance is shown in Figs. 30 and 31. The goal of this study was to use non-intrusive optical diagnostics to observe transitional SWBLI (XSWBLI), which are not as well documented in literature as laminar and turbulent SWBLI. Unprecedented high-speed pressure-sensitive paint measurements were combined with high-speed schlieren, IR thermography, and oil flow visualization to study the XSBLI. Recent testing in the 31-Inch Mach 10 Air Tunnel in 2022 also included multi-point focused laser differential interferometry (FLDI) and high-speed self-aligned focusing schlieren (SA-FS), see Fig. 32, diagnostics that provided data which can be compared to high-speed surface-mounted pressure-transducer data. The experimental results provide a clearer picture of the structure of the flow field in the interaction region due to a transitional incoming boundary layer, which can affect thermal and acoustic loading and flight control of vehicles.

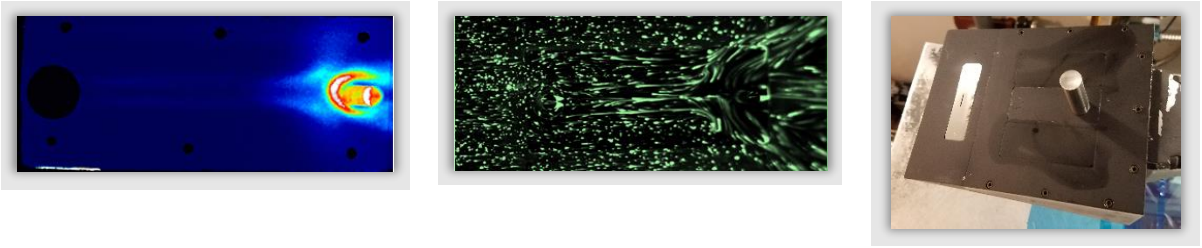

a) b) c)

Fig. 30 a) High-speed pressure sensitive paint and b) oil flow data on c) a flat plate model with a protruding cylinder [Photo Source: NASA].

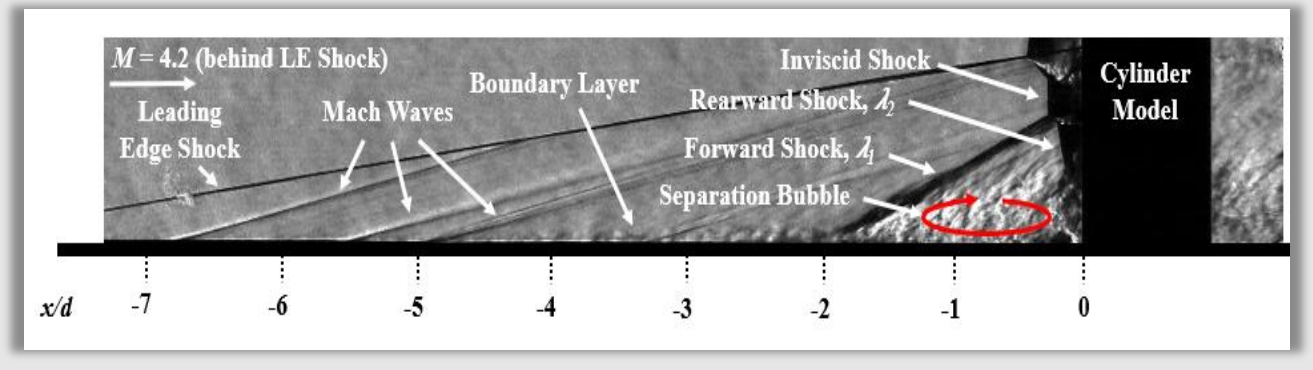

Fig. 31 Schlieren photograph and diagram of SWBLI on flat plate with cylinder.

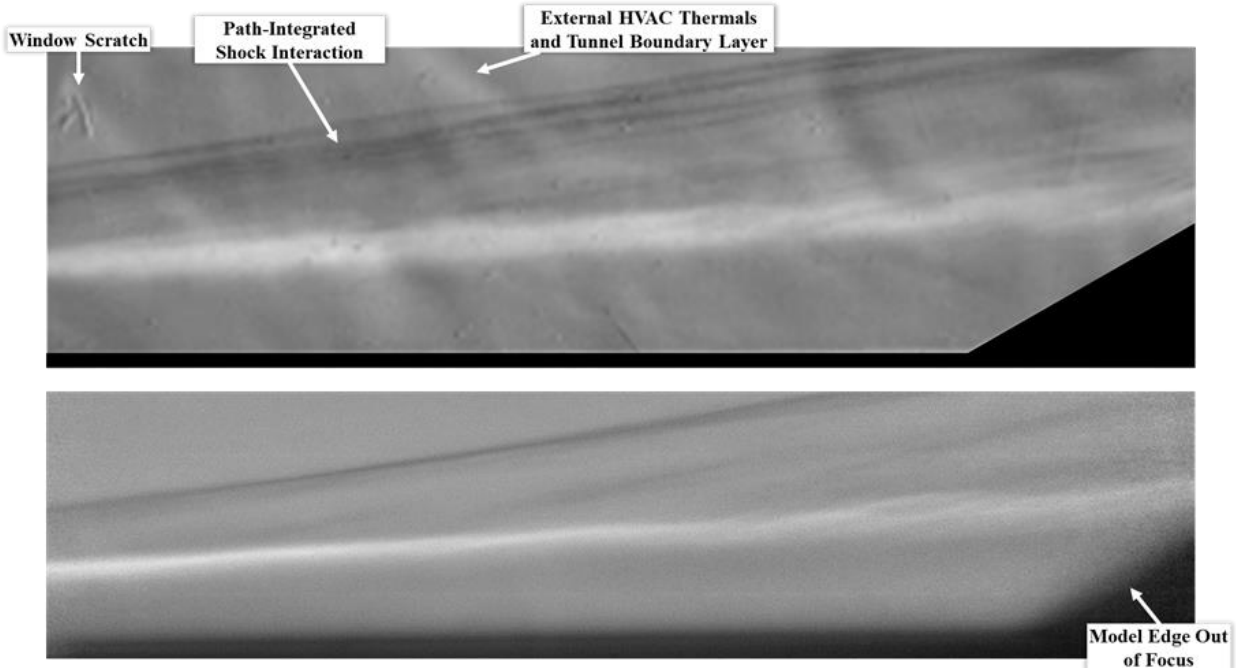

Fig. 32 Conventional high-speed schlieren (top) compared to self-aligned focusing schlieren system (bottom) with a ramp shock generator.

VII. Test Technique Development

Novel aeroheating and flow field visualization techniques are under development for use in the LAL. A few examples of these techniques are described in the following sections.

A. Higher Temperature Phosphor Thermography

The maximum temperature that the standard two-color phosphor thermography (STCP) system can measure is 338°F (170°C). Leading edges, control surfaces, and other features on ceramic models will quickly exceed this maximum temperature in the 31-Inch Mach 10 Air Tunnel and may exceed that temperature at higher Reynolds number conditions in the 20-Inch Mach 6 Air Tunnel. To avoid such overscaling, new phosphors and imaging systems are being developed and tested in LAL facilities that can double the temperature range and reduce measurement uncertainty of this technique. A new higher-temperature phosphor thermography (HTT2) coating has been formulated and is under evaluation that will increase the maximum temperature measurement to 608°F (320°C). Figure 33 shows HTT2 emission spectra with temperature. A typical 3-detector color camera with a dichroic prism filter was used previously to provide color responsivities. While this type of camera worked for the STCP system, the overlap between the red and green responsivities greatly reduces the sensitivity of the HTT2 system. Therefore, a multispectral camera with a neutral splitting prism and custom detector filters is being developed which completely separates color responsivities. A comparison of the two camera systems is shown in Fig. 34. Using the multispectral camera system reduces the temperature measurement uncertainty by 50% for HTT2, across the temperature range, and by 25% for STCP, at lower temperatures, as shown in Fig. 35.

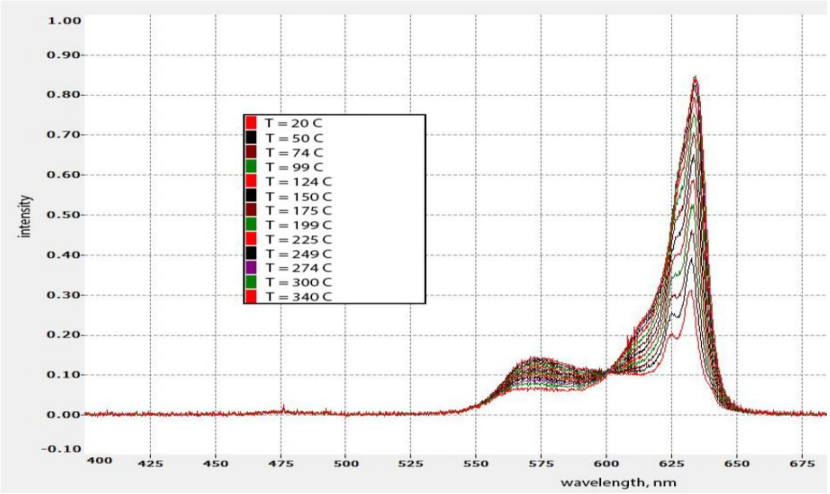

Fig. 33 HTT2 Emission Spectra with Temperature.

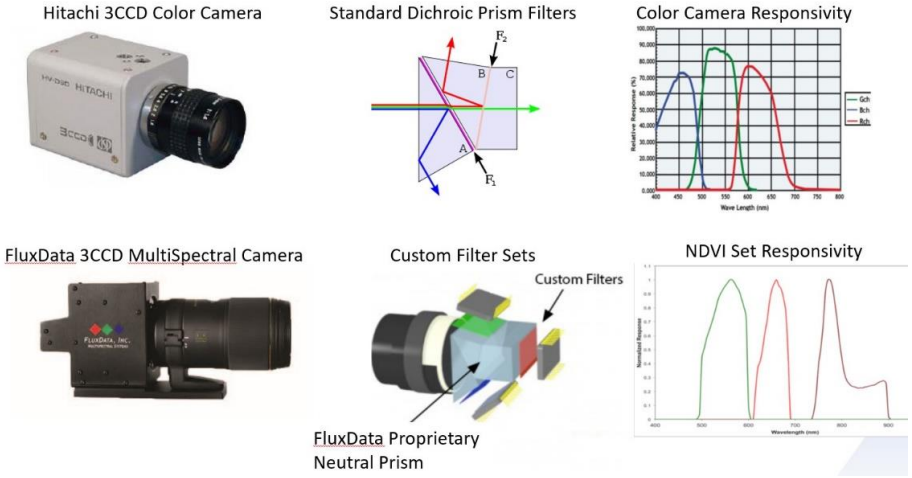

Fig. 34 Comparison of 3-Detector Color (Dichroic) and Multi-Spectral (NDVI) Cameras.

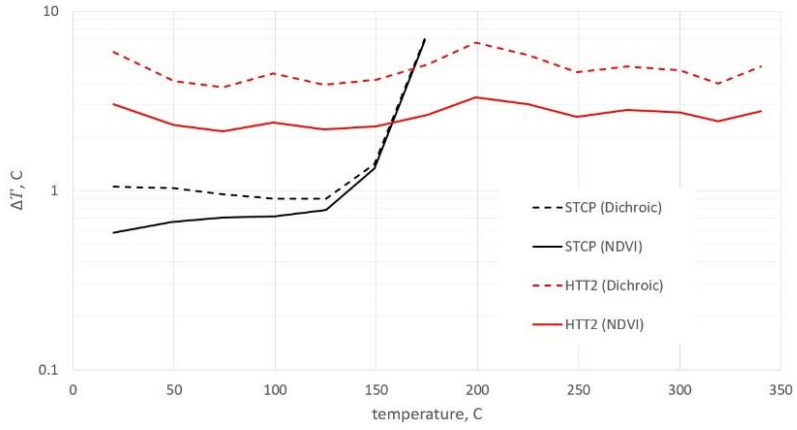

Fig. 35 Comparison of Temperature Measurement Uncertainties.

B. Mid-Wave Infrared Thermography

A quantitative IR thermography technique is being developed to acquire aeroheating data on geometries where traditional global techniques do not perform well. Traditional global techniques such as phosphor thermography and temperature-sensitive paint can easily overscale in regions of high heating on sharp leading edges or blunt bodies, or uncertainty can be unacceptably high in cases of low heating on slender geometries. Modern IR cameras solve both problems via tunable integration times and super-framing capabilities to extend the dynamic range.

Implementation of a quantitative IR technique is difficult due to the need to correct for directional emissivity and ambient reflections. A validation test campaign was developed to address these obstacles and drive down measurement uncertainties. An initial test entry with PEEK and cast ceramic hemispheres was completed in January 2024. Follow-on tests will look at geometries with complex flow fields and challenging fields of view, such as aeroshell and aftbody heating.

A high-resolution mid-wavelength (MWIR) camera was purchased, and the tunnel optical access was upgraded, to permit measurements in both long-wavelength (LWIR) and MWIR bandwidths. The cameras are radiometrically calibrated in reference to a NIST-traceable cavity blackbody and corrections for transmission losses through the window are addressed via in-situ calibrations. A spatial calibration of the camera-lens system is also performed to obtain camera extrinsic and intrinsic parameters for accurate 3-D mapping and directional emissivity correction. The current capability development effort was tailored primarily for the 20-Inch Mach 6 Air Tunnel. Additional efforts will extend the capability for measurements at the 31-Inch Mach 10 Air Tunnel which has significantly higher stagnation heating rates necessitating a higher dynamic range of the IR thermography technique.

C. Energy-Matter Interaction Diagnostics for Hypersonics

Researchers from the Lawrence Livermore National Laboratories (LLNL) have developed in-situ optical diagnostics to measure energy-matter interactions in hypersonic flow and have partnered with NASA LaRC to obtain validation data for the new tools. The test objective was to evaluate those diagnostics techniques in wind tunnel testing environments.

These diagnostics had previously been used only in static chambers to assess damage from energy interactions, such as laser weapons. LLNL is working to upgrade the diagnostic capability to function in supersonic and hypersonic flow environments. These techniques are well established in the literature for high-fidelity static non-destructive measurements but have never been used in wind tunnel environments. Vibrations of the tunnel along with unsteady airflow and optical distortions from boundary layers and shocks could create sufficient disturbances to render the techniques ineffective.

The primary techniques tested in the LAL 31-Inch Mach 10 Air Tunnel were laser-based ultrasonics (LBU) [56] in which a vibration measurement taken at a short distance from its source is used to measure in situ changes in material properties, such as density and porosity, and laser speckle interferometry (LSI) [57] which measures small changes in surface displacement such as strain. LBU was tested in two configurations: one using a piezo device under the test sample to excite vibrations (Fig. 36), and the other using a laser to ping the surface (fully optical non-contact measurement, as in Fig. 37). LLNL successfully measured signal on both a stainless-steel sample, statically and under rigid body motion, as well as on a more challenging gold-coated graphite sample, which is significantly more porous and more closely simulates vehicle materials of relevance. LSI was tested on a flush graphite sample and measured no net movement, as expected. The sample then was raised off the surface a few millimeters to add heating from the step edge and a small amount of strain was detected. Both LBU and LSI techniques were adapted for wind-tunnel test sections and shown to be viable in hypersonic testing environments.

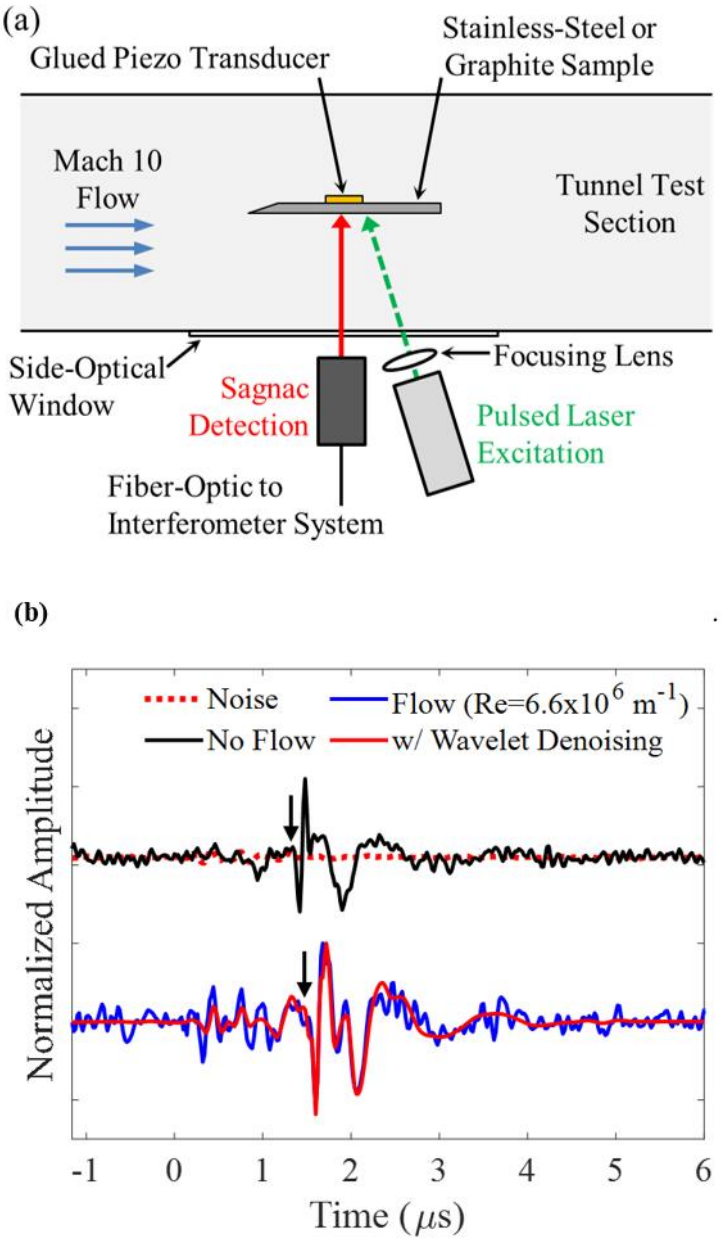

Fig. 36 a) Diagram of LBU setup in Mach 10 tunnel and b) averaged time traces with LBU of optical detection with pulsed laser excitation on steel before and during flow with a trip strip.

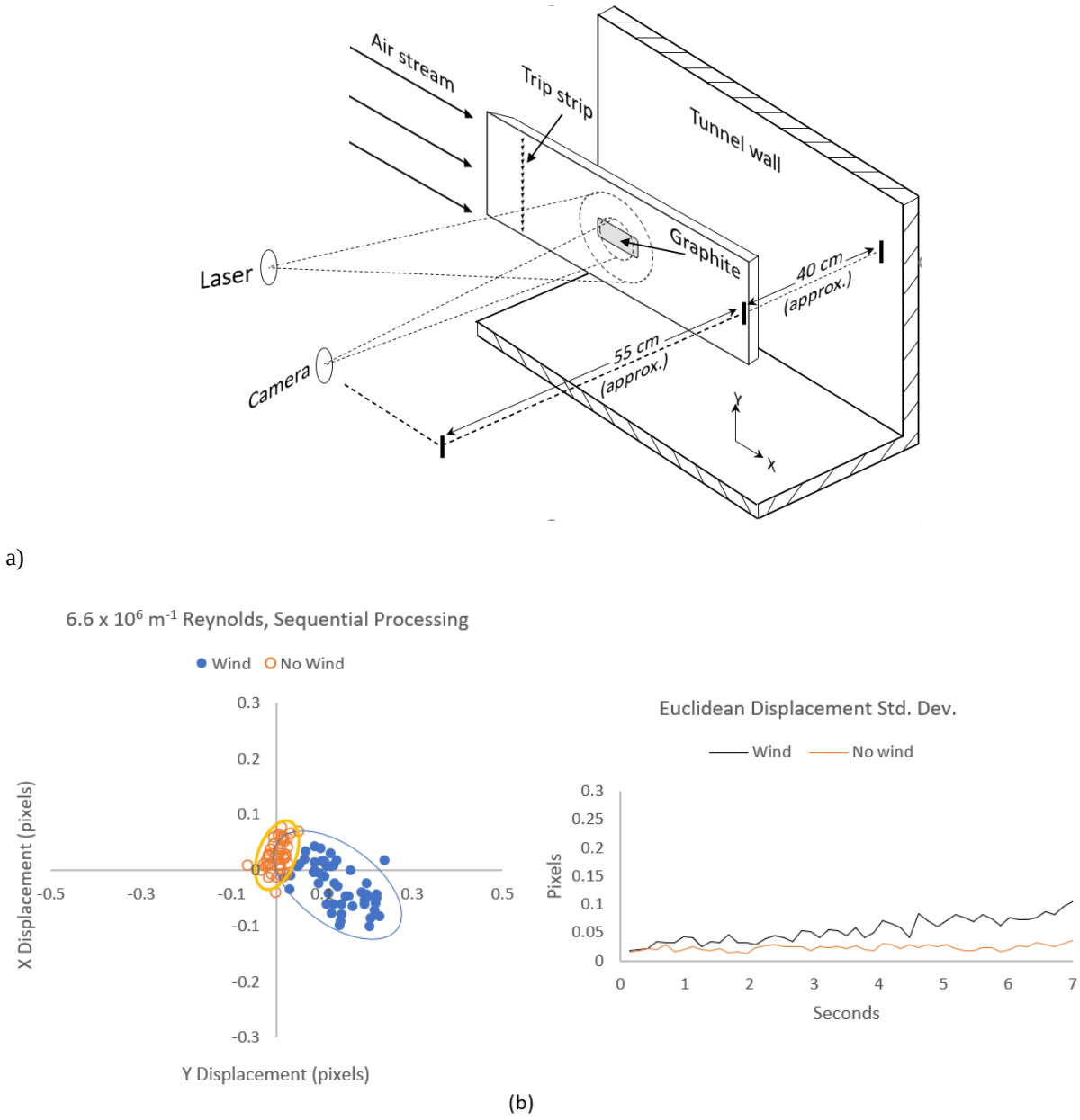

Fig. 37 a) Experimental layout of LSI setup in Mach 10 tunnel wind tunnel and b) displacement results computed from surface-focused speckle pattern during flow with a trip strip.

D. Planar Laser-induced Fluorescence

Planar laser-induced fluorescence (PLIF) measurements of seeded nitric oxide was performed in November 2022 at the Mach 10 tunnel to visualize planar slices in the wake of a wind tunnel model relevant to the LOFTID flight program [58]. An overview of PLIF measurements performed at the 31-in Mach 10 tunnel is provided in a recent review paper by Danehy *et al*. [59]. Examples of 2D PLIF flow visualization images from the recent test are shown in Fig. 38 at freestream conditions corresponding to a) $Re_\infty = 0.55x10^6$ ft^{-1} and b) $Re_\infty = 1.92x10^6$ ft^{-1}. The PLIF measurement technique can provide off-body measurements with a spatial resolution within 1 mm and a temporal resolution within 1 μs and is typically performed at a repetition-rate of 10 Hz. Quantitative metrics such as the location of shocks and other flow features of interest can be measured from a spatially calibrated 2D PLIF image and

directly compared with CFD solutions. Dedicated wind tunnel runs to measure velocity and temperature in the wake were also completed for the LOFTID-relevant model and data analysis is in-progress. A representative 2D-1C (two dimensional, one-component) velocity field using molecular tagging velocimetry is provided in Fig. 39at Re_∞ = $0.55x10^6$ ft^{-1}, which shows the z-direction velocity field in the wake [60]. Another means of comparing experimental PLIF measurements to CFD solutions is by generating a synthetic PLIF image through modeling the PLIF signal intensity using the spectroscopic properties of the laser-induced fluorescence process and calculated thermodynamic properties from CFD solutions [61]. While the recent wind tunnel test entry was performed at a repetition rate of 10 Hz, a high-speed PLIF system developed through an SBIR with Spectral Energies, LLC is now available for use at NASA Langley to perform high-speed flow visualization, velocimetry [62, 63], and quantitative multi-parameter measurements [64].

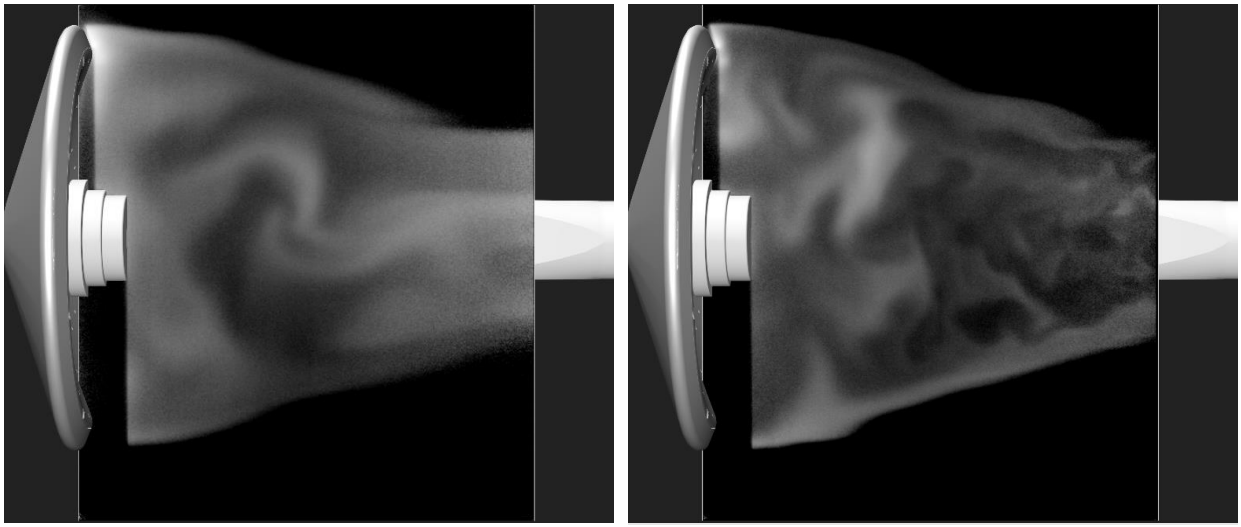

a) **b)**

Fig. 38 Example PLIF images showing the wake structure for a LOFTID-relevant wind tunnel model at conditions corresponding to a) Re_∞ = 0.55 x 10^6 ft^{-1} and b) Re_∞ = 1.92 x 10^6 ft^{-1}.

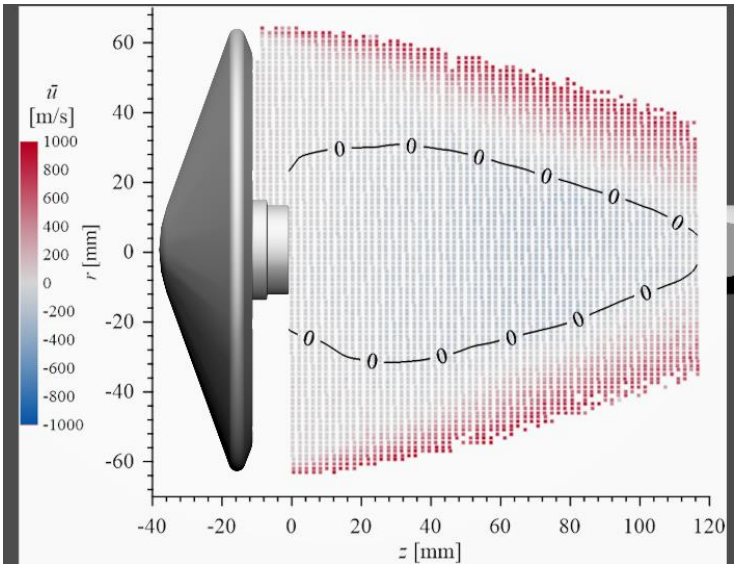

Fig. 39 Example time-averaged streamwise velocity using PLIF molecular tagging velocimetry for a LOFTID-relevant wind tunnel model at conditions corresponding to Re_∞ = 0.55 x 10^6 ft^{-1} [60R2].

E. Femtosecond Laser Electronic Excitation Tagging Velocimetry

Velocity measurements were also recently performed at the Mach 10 tunnel for the unseeded air using the femtosecond laser electronic excitation tagging (FLEET) technique. FLEET velocimetry has been applied to a variety of flow conditions in the literature as recently reviewed by Danehy *et al*. [65], although very limited work is current available for FLEET at hypersonic low-pressure air conditions. Over two different test campaigns, FLEET measurements were performed for velocimetry in the wake of the LOFTID-relevant model (December 2022) and in the tunnel freestream (January 2023) using a commercially available 1 kHz ultrafast (femtosecond) laser system and an ultrahigh-speed intensified camera system. Notably, the FLEET measurements performed during this effort were the first direct measurement of freestream velocity at this hypersonic wind tunnel facility. For the experimental arrangement used at the Mach 10 tunnel (described in [60]), the generated FLEET signal was a short (~ 2 mm) tagged line that was tracked for 1C velocimetry. A sequence of three time-averaged FLEET images at the tunnel centerline are shown in Fig. 40 for Re_∞ = 0.55 x 10^6 ft^{-1}, with the velocity determined from the measured displacement and the known time interval between the images. Instantaneous velocity at the wind tunnel centerline for Re_∞ = 0.55 x 10^6 ft^{-1} is shown in Fig. 41 a) for a recording length of 5 seconds, while the instantaneous streamwise velocity in the wake of the LOFTID-relevant model for a recording length of 10 seconds is shown in Fig. 41b) for the Re_∞ = 0.55 x 10^6 ft^{-1} condition and at a measurement location corresponding to ~12 mm from the payload at the model centerline.

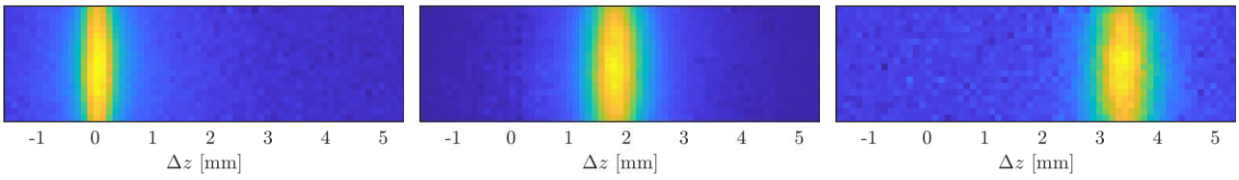

a) **b)** **c)**

Fig. 40 Average freestream FLEET images at the Mach 10 wind tunnel centerline used to measure velocity through the displacement and time interval: a) image centered at t = 0 µs, b) 1st delay image centered at t = 1.27 µs, c) and 2nd delay image centered at t = 2.41 µs [60].

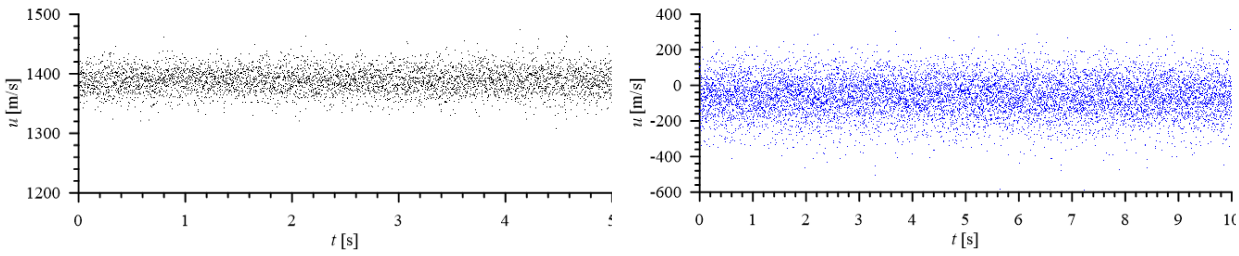

a) **b)**

Fig. 41 Instantaneous FLEET measurements of: a) freestream centerline streamwise velocity and b) wake centerline streamwise velocity [60].

VIII. Facility Calibrations

Flow field calibrations are performed regularly using flow rakes that feature interchangeable probes and can be used for measurements of mean and fluctuating pressures, total temperature, and mass flux. Instrumentation calibrations also are performed for LAL measurement techniques such as the phosphor thermography system.

A. Freestream disturbance rake

Freestream disturbances were measured using a flow rake in two separate 20-Inch Mach 6 Tunnel test entries. The flow rake measurements from the second entry in 2019 corroborated measurements from the 2017 entry reported in Ref. 66. The rake was instrumented with Kulite and PCB high-bandwidth pressure transducers and with hot-wire anemometers to quantify pressure and mass flux fluctuations, respectively. The unit Reynolds number range was varied from 1.0-8.1 x 10^6 /ft. Normalized total pressure fluctuations ranged from 0.84% at the highest Re_∞ to 1.89% at the lowest Re_∞. Mass-flux fluctuations showed less dependence on freestream Re and ranged from 1.8-2.5%. Simultaneous FLDI measurements and high-speed schlieren images were also acquired in the later test entry [67].

B. Flow survey measurements

Measurements of the test section flow in LAL facilities are performed using the LAL Flow Survey Rake. This pressure rake, built in 2014, contains 31 pitot probes of 0.083 inches in diameter, spaced at 0.5 inches between probe centers, thus spanning a total of 15 inches of the test section flow field. The rake is designed for adjustments to axial position in 2.5-inch increments as well as changes to the roll orientation in 15-deg increments using a clutch face arrangement. The probes are designed for easy removal in case of damage or to install different types of probes such as high-frequency pressure fluctuation probes or static pressure probes. Soft pressure tubing connections are made to the probes inside of the rake body, and all interior surfaces of the stainless-steel rake and strut are lined with insulating thermoplastic to protect the tubing from high temperatures encountered in the hypersonic facilities. Rake pressures are typically measured using electronically scanned pressure (ESP) modules located out of the flow, at the base of the strut, to minimize pneumatic lag in the pressure measurements. A photograph of the rake installed in a vertical orientation on the model support system for the 31-Inch Mach 10 Air Tunnel is shown in Fig. 42.

Flow surveys have ranged from short tests to investigate flow features or phenomena to full calibrations using compact, efficient experiments developed using formal design of experiments methods [68]. Test section total temperature distributions are measured using a separate total temperature rake that employs 19 0.25-inch-diameter, aspirated, double-shielded total temperature probes spaced at 1-inch intervals between probe centers. The probes utilize bare-bead Type-K thermocouples for the temperature measurements. A photograph of the total temperature rake is shown in Fig. 43

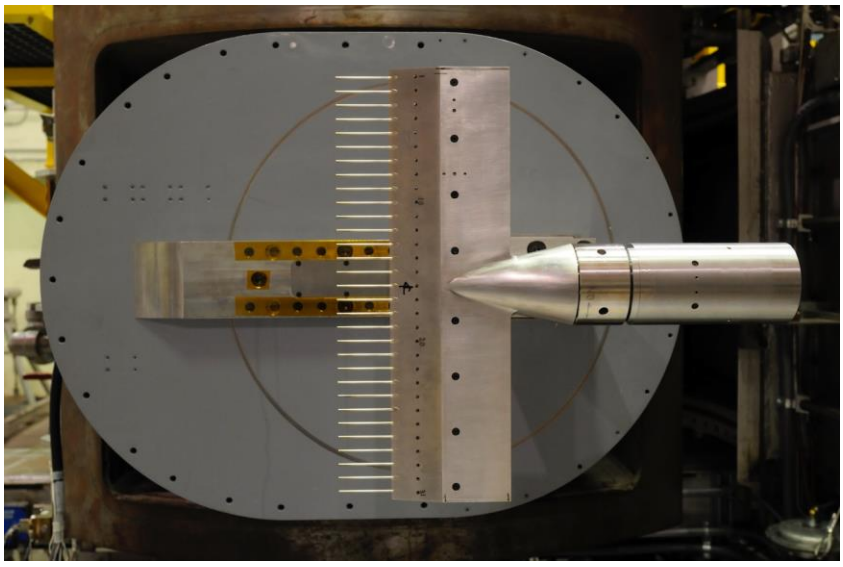

Fig. 42 Flow Survey Rake Installed on the 31-Inch Mach 10 Air Tunnel Model Support System. [Photo Source: NASA]

Fig. 43 LAL Total Temperature Rake. [Photo Source: NASA]

C. Phosphor thermography check standard

Phosphor thermography tests follow calibrations using hemisphere stagnation heating as an aeroheating check standard configuration. Data acquired across a range of Reynolds numbers on a smooth, 4-inch-diameter hemisphere, or hemisphere-cylinder, model are compared to previous results and computational predictions to validate the computed heating measurements from each batch of phosphor coating the LaRC Aerothermodynamics Branch fabricates. The analytical peak heating on the hemisphere is approximately unity with respect to Fay-Riddell [69]. Additional check standard tests are conducted periodically to monitor the overall performance of the system. These tests are performed to check the stability of the phosphor coating, the cameras and UV lights being used, and the wind tunnel window.

IX. Summary

A review has been presented of the Langley Research Center Aerothermodynamic Laboratory experimental capabilities that support flight programs, foundational research and development activities, academic partnerships, and facility calibrations. Facility operating characteristics, model fabrication capabilities and measurement techniques were discussed. Recent (2017-2024) contributions to major NASA flight programs and to research and development activities were summarized. These capabilities have been, and will continue to be, applied to flight database generation, configuration development, CFD benchmarking and fundamental studies of complex aerothermodynamic phenomena.

X. Acknowledgement

The authors appreciate the contributions from several individuals and groups who supported the testing described in this paper. The authors specifically wish to thank: Mark Cagle, Robert Andrews, Michael Powers, and Clinton Reese for their assistance in model design, fabrication and preparation; Kevin Hollingsworth, Nicholas Shaw, Joe Rodriguez, Johnny Ellis, Anthony Robbins, Jonathan Crider, Stanley Barnett for wind tunnel support; Kevin Hollingsworth, Sheila Wright and Tina Reynolds for data acquisition assistance; Gregory Brauckmann for leading test campaigns and assistance in data interpretation and understanding; Paul Danehy, Olivia Tyrrell, and Joshua Weisberger for contributions towards application of the various diagnostics discussed; and Sarah Agam, Frank Greene, and William Wood for LAURA computations. Without their help, conducting these tests and compiling these data sets would not have been possible.

XI. References

1. Hollis, B. R., Berger, K. T., Berry, S. A., Brauckmann, G. J., Buck, G. M., DiFulvio, M., Horvath, T. J., Liechty, D. S., Merski, N. R., Murphy, K. J., Rufer, S. J., and Schoenenberger, M., "Entry, Descent, and Landing Aerothermodynamics: NASA Langley Experimental Capabilities and Contributions," AIAA Paper 2014-1154, January 2014. https://doi.org/10.2514/6.2014-1154

2. Berry, S. A. and Berger, K. T., "NASA Langley Experimental Aerothermodynamic Contributions to Slender and Winged Hypersonic Vehicles," AIAA Paper 2015-0213, *53rd AIAA Aerospace Sciences Meeting*, Kissimmee, FL, 5-9 January 2015. https://doi.org/10.2514/6.2015-0213

3. Berger, K. T., Hollingsworth, K. E., Wright, S. A., and Rufer, S. J., "NASA Langley Aerothermodynamics Laboratory: Hypersonic Testing Capabilities," AIAA Paper 2015-1337, *53rd AIAA Aerospace Sciences Meeting*, Kissimmee, FL, 5-9 January 2015. https://doi.org/10.2514/6.2015-1337

4. Buck, G. M., "Rapid Model Fabrication and Testing for Aerospace Vehicles," AIAA Paper 2000-0086, *38th Aerospace Sciences Meeting and Exhibit*, Reno, NV, January 10-13, 2000. https://doi.org/10.2514/6.2000-826

5. Mason, M. L., and Rufer, S. J., "Imaging for Hypersonic Experimental Aeroheating Testing (IHEAT) version 4.3: User Manual," NASA/TM-20210021999, October 2021.

6. Buck, G. M., "Automated Thermal Mapping Techniques Using Chromatic Image Analysis," NASA TM-101554, April 1989.

7. Merski, N. R., "Global Aeroheating Wind-Tunnel Measurements Using Improved Two-Color Phosphor Thermography Method," *Journal of Spacecraft and Rockets*, Vol. 36, No. 2, March 1999, pp. 160-170. https://doi.org/10.2514/2.3446

8. Zacarra, M., Edlelman, J. B., and Cardone, G., "A General Procedure for Infrared Thermography Heat Transfer Measurements in Hypersonic Wind Tunnels," International Journal of Heat and Mass Transfer, Vol. 163, 2020, pp. 1-16. https://doi.org/10.1016/j.ijheatmasstransfer.2020.120419

9. Watkins, A. N., Buck, G. M., Leighty, B. D., and Lipford, W. E., "Using Pressure- and Temperature-Sensitive Paint for Global Surface Pressure and Temperature Measurements on the Aft-Body of a Capsule Reentry Vehicle" AIAA Paper 2008-1230, *46th AIAA Aerospace Sciences Meeting and Exhibit*, Reno, NV, 7-10 January 2008. https://doi.org/10.2514/6.2008-1230

10. Buck, G. M., Watkins, A. N., Danehy, P. M., Inman, J. A., Adlerfer, D..W., and Dyakonov, A. A., "Experimental Measurement of RCS Jet Interaction Effects on Capsule Reentry Vehicle," AIAA Paper 2008-1229, *46th AIAA Aerospace Sciences Meeting and Exhibit*, Reno, NV, 7-10 January, 2008. https://doi.org/10.2514/6.2008-1229

11. Horvath, T. J., Berry, S. A., Merski, N. R., and Fitzgerald, S. M., "X-38 Experimental Aerothermodynamics," *Journal of Spacecraft and Rockets*, Vol. 41, No. 2, March-April 2004, pp. 272-292. https://doi.org/10.2514/1.9198

12. Horvath, T. J., Berry, S. A., Hollis, B. R., Chang, C., and Singer, B. A., "Boundary Layer Transition on Slender Cones in Conventional and Low Disturbance Mach 6 Wind Tunnels," AIAA Paper 2002-2743, *32nd AIAA Fluid Dynamics Conference and Exhibit*, St. Louis, MO, 24-26 June 2002. https://doi.org/10.2514/6.2002-2743

13. Horvath, T. and Hannemann, K., "Blunt Body Near-Wake Flow Field at Mach 10," AIAA Paper 1997-0986, *35th AIAA Aerospace Sciences Meeting and Exhibit*, Reno, NV, 6-9 January 1997. https://doi.org/10.2514/6.1997-986

14. Schultz, D. L. and Jones, T. V., "Heat-Transfer Measurements in Short-Duration Facilities," AGARD Report AG-165, February 1973.

15. Hollis, B. R., "User's Manual for the One-Dimensional Hypersonic Aero-Thermodynamic (1DHEAT) Data Reduction Code," NASA CR 4691, August 1995.

16. Rufer, S. J. and Berridge, D. C., "Experimental Study of Second-Mode Instabilities on a 7-Degree Cone at Mach 6," AIAA Paper 2011-3877, *41st AIAA Fluid Dynamics Conference and Exhibit*, Honolulu, HI, 27-30 June 2011. https://doi.org/10.2514/6.2011-3877

17. Murphy, K. J. and Scallion, W. I., "Experimental Stage Separation Tool Development in NASA Langley's Aerothermodynamics Laboratory," AIAA Paper 2005-6127, AIAA *Atmospheric Flight Mechanics Conference and Exhibit*, San Francisco, CA, 15-18 August 2005. https://doi.org/10.2514/6.2005-6127

18. Bathel, B. F., Johansen, C., Inman, J. A., Jones, S. B., and Danehy, P. M., "Review of Fluorescence-Based Velocimetry Techniques to Study High-Speed Compressible Flows," AIAA Paper 2013-0339, *51st AIAA Aerospace Sciences Meeting*, 7-10 January 2013. https://doi.org/10.2514/6.2013-339

19. Danehy, P. M., Wilkes, J. A., Alderfer, D. W., Jones, S. B., Robbins, A. W., Patry, D. P., and Schwartz, R. J., "Planar Laser-Induced Fluorescence (PLIF) Investigation of Hypersonic Flow Fields in Mach 10 Wind Tunnel," AIAA Paper 2006-3442, *25th AIAA Aerodynamic Measurements Technology and Ground Testing Conference*, San Francisco, CA, 5-8 June 2006. https://doi.org/10.2514/6.2006-3442

20. Rhode, M. N. and DeLoach, R., "Hypersonic Wind Tunnel Calibration Using the Modern Design of Experiments", AIAA Paper 2005-4274, *41st AIAA/ASME/SAE/ASEE Joint Propulsion Conference & Exhibit*, Tucson, AZ, 10-13 July 2005. https://doi.org/10.2514/6.2005-4274

21. Rufer, S. J. and Berridge, D. C., "Pressure Fluctuation Measurements in the NASA Langley 20-Inch Mach 6 Air Tunnel," AIAA Paper 2012-3262, *42nd AIAA Fluid Dynamics Conference and Exhibit*, 25-28 June 2012. https://doi.org/10.2514/6.2012-3262

22. Gnoffo, P. A., "An Upwind-Biased, Point-Implicit Algorithm for Viscous, Compressible Perfect-Gas Flows," NASA TP-2953, February 1990.

23. Thompson, K. B. Hollis, B. R., Johnston, C. O., Kleb, B. L, Lessard, V. R. and Mazaheri, A., "LAURA User's Manual: 5.6," NASA TM-2020-220566, February 2020.

24. Biedron, R. T., Carlson, J., Derlaga, J. M., Gnoffo, P. A., Hammond, D. P., Jones, W. T., Kleb, B., Lee-Rausch, E. M., Nielsen, E. J., Park, M. A., Rumsey, C. L., Thomas, J. L., Thompson, K. B., and Wood, W. A., "FUN3D Manual: 13.5," NASA TM-2019-220271, April 2019.

25. Chang, C.-L., "The Langley Stability and Transition Analysis Code (LASTRAC) Version 1.2 User Manual," NASA TM-2004-213233, June 2004.

26. Liechty, Derek S., "Aerothermodynamic Testing of Protuberances and Penetrations on the NASA Cycle I Crew Exploration Vehicle Heat Shield in the NASA Langley 20-Inch Mach 6 Air Tunnel.: Test 6918," NASA EG-CAP-06-155, November, 2006.

27. Hollis, Brian R., "Compression Pad Cavity Heating Augmentation on Orion and Heat Shield," *Journal of Thermophysics and Heat Transfer*, Vol.25, Issue 3, Jul/Sep 20-11, pp. 329-340. https://doi.org/10.2514/1.48076

28. Edquist, K. T., Hollis, B. R., Johnston, C. O., and Bose, D., "Mars Science Laboratory Heatshield Aerothermodynamics: Design and Reconstruction," AIAA Paper 2013-2781, *44th AIAA Thermophysics Conference*, San Diego, CA, 24-27 June 2013. https://doi.org/10.2514/6.2013-2781

29. Hollis, B. R., Wise, A. J., Liechty, D. S., Korzun, A. M., Thompson, K. B., Rodrigues, N. S. and Rieken, E. F., "Aerothermodynamic Analyses for the LOFTID Technology Demonstration Mission," AIAA Paper 2024-1498, *AIAA SciTech 2024 Forum*, Orlando, FL, January 8-2, 2024. https://doi.org/10.2514/6.2024-1498

30. Wheaton, B. M., Butler, C. S., McKiernan, G. R., and Berridge, D. C., "Initial Results from the BOLT Flight Experiment," AIAA Paper 2022-0345, AIAA SciTech 2022 Forum, San Diego, CA, 3-7 January 2022. https://doi.org/10.2514/6.2022-0345

31. Wirth, J., Morrelae, B., Kostak, H., Bowersox, R., Dufrene, A., Portoni, P., and Wadhams, T., "Boundary Layer Turbulence Flight Experiment in Memory of Mike Holden: Side A Flight Results," AIAA Paper 2023-0682, *AIAA SciTech 2023 Forum*, National Harbor, MD, 23-27 January 2023. https://doi.org/10.2514/6.2023-0682

32. Berry, S. A. and Wheaton, B. M., "BOLT II Roughness Side Flight Results," AIAA Paper 2023-0684, *AIAA SciTech 2023 Forum*, National Harbor, MD, 23-27 January 2023. https://doi.org/10.2514/6.2023-0684

33. Berry, S. A., Mason, M. L., Greene, F. A., King, R. A., Rieken, E. F., and Basore, K. D., "LaRC Aerothermodynamic Ground Tests in Support of BOLT Flight Experiment," AIAA Paper 2019-0091, *AIAA SciTech 2019 Forum*, San Diego, CA, 7-11 January 2019. https://doi.org/10.2514/6.2019-0091

34. Rieken, E. F., Berry, S. A., Broslawski, C. J., and Greene, F. A., "Aeroheating Measurements of BOLT Aerodynamic Fairings and Transition Module," AIAA 2020-1561, *AIAA SciTech 2020 Forum*, Orlando, FL, 6-10 January 2020. https://doi.org/10.2514/6.2020-1561

35. Berry, S. A., Scott, C. F., Broslawski, C. J., Turbeville, D., and Greene, F. A., "Recent BOLT Discrete-Roughness Trip Results from the 20-Inch Mach 6 Air Tunnel," AIAA Paper 2023-0086, *AIAA SciTech 2023 Forum*, National Harbor, MD, 23-27 January 2023. https://doi.org/10.2514/6.2023-0086

36. Berry, S. A. and Scott, C. F., "Experimental Aeroheating Study in NASA LaRC 20-Inch Mach 6 Air Tunnel: Test 7071 Discrete Roughness on BOLT," NASA TM-20230003164, April 2023.

37. Cheatwood, J., Johnston, C. O., and Hollis, B. R., "Mars Sample Return Earth Entry System Woven Roughness Mach 6 Aeroheating Test," AIAA Paper 2024-0443, *AIAA SciTech 2024 Forum*, Orlando, FL, January 2024. https://doi.org/10.2514/6.2024-0443

38. Reshotko, E. and Tumin, A., "Role of Transient Growth in Roughness-Induced Transition," *AIAA Journal*, Vol. 42, No. 4, 2004, pp. 766-770. https://doi.org/10.2514/1.9558

39. Sousa, C. E., Kennedy, R. E., King, R. A., Bathel, B. F., Weisberger, J. M., and Laurence, S. J., "Global analysis of nonlinear second-mode development in a Mach-6 boundary layer from high speed schlieren data," Experiments in Fluids [online journal], Vol. 65, No. 19, URL: https://doi.org/10.21203/rs.3.rs-2366613/v1 [retrieved 31 May 2024].

40. Bathel, B. F., Weisberger, J. M., Herring, G. C., King, R. A., Jones, S. B., Kennedy, R. E., and Laurence, S. J., "Two-point, parallel-beam focused laser differential interferometry with a Nomarski prism," *Appl Opt.* [online journal], Vol. 59, No. 2, pp. 244-252, URL:https://pubmed.ncbi.nlm.nih.gov/32225301/ [retrieved 31 May 2024].

41. Leidy, A., King, R. A., and Chou, A., "Bluntness and Supersaturation Effects on the Second Mode Instability in Mach 10 Flow", AIAA Paper 2021-2876, *AIAA Aviation 2021 Forum*, Virtual Event, 2-6 August 2021. https://doi.org/10.2514/6.2021-2876

42. Leidy, A., King, R., Choudhari, M. M., and Paredes, P., "Hypersonic Second Mode Instability Response to Shaped Roughness", AIAA Paper 2021-0149, *AIAA SciTech 2021 Forum*, 11-15 & 19-21, Virtual Event, January 2021. https://doi.org/10.2514/6.2021-0149

43. Hollis, B. R., "Experimental Investigation of Hexcomb-Pattern Roughness Effects on Transition Onset and Turbulent Heating Augmentation at Mach 6," NASA/TM-2019-220424, November 2019.

44. Hollis, B. R. and Hollingsworth, K. E., "Experimental Investigation of Distributed Sand-Grain Roughness Effects on Transition Onset and Turbulent Heating Augmentation at Mach 6," NASA/TM-2022-0005643 (Revision 1), February 2013.

45. Hollis, B. R. and Hollingsworth, K. E., "Experimental Investigation of Block-TPS Fence/Gap Roughness Effects on Transition Onset and Turbulent Heating Augmentation at Mach 6," NASA/TM-2023-0001707 (Revision 1), April 2013.

46. Oberkampf, W.L., Aeschliman, D.P., Tate, R.E., and Henfling, J.F., "Experimental Aerodynamics Research on a Hypersonic Vehicle", Sandia Report SAND92-1411, April 1993.

47. Chynoweth, B. C., Edelman, J. B., Gray, K. A., McKiernan, G. R., and Schneider, S. P., "Measurements in the Boeing/AFOSR Mach-6 Quiet Tunnel on Hypersonic Boundary-Layer Transition," AIAA Paper 2017-3632, *47th AIAA Fluid Dynamics Conference*, Denver, CO, 5-9 June 2017.

48. Draper, J. W., Brauckmann, G. J., Turbeville, F. D. and Lee, S. W., "Dynamic Force Reconstruction of Transient Flap Control Force Experiments in a Hypersonic Wind Tunnel," AIAA Paper 2024-2661, *AIAA SciTech 2024 Forum*, Orlando, FL, 8-12 January 2024. https://doi.org/10.2514/6.2024-2661

49. Korzun, A. M., K. J. Murphy, and K. T. Edquist, "Supersonic Aerodynamic Characteristics of Blunt Body Trim Tab Configurations", AIAA Paper 2013-2809, *31st AIAA Applied Aerodynamics Conference*, San Diego, CA, 24-27 June 2013. https://doi.org/10.2514/6.2013-2809

50. Murphy, K. J., Watkins, A. N., Korzun, A. M., and Edquist, K. T., "Testing of the Trim Tab Parametric Model in NASA Langley's Unitary Plan Wind Tunnel," AIAA Paper 2013-2308, *31st AIAA Applied Aerodynamics Conference*, San Diego, CA, 24-27 June 2013. https://doi.org/10.2514/6.2013-2808

51. Turbeville, D. and Schneider, S., "Effect of Freestream Noise on Fin-Cone Transition at Mach 6," AIAA Paper 2022-3857, *AIAA Aviation 2022 Forum*, Chicago, IL, June 27 – July 1, 2022. https://doi.org/10.2514/6.2022-3857

52. Schöneich, A. G., McQuaid, J. A., Laurence, S. J., Dettenrieder, F., Bodony, D. J., Buck, G. M., Weisberger, J. M., and Bathel, B. F., "Hypersonic Fluid-Thermal-Structural Interactions on a Compression Ramp with an Embedded Compliant Panel," AIAA Paper 2023-3851, *AIAA Aviation 2023 Forum*, San Diego, CA, 12-16 June 2023. https://doi.org/10.2514/6.2023-3851

53. Whalen, T. J., Schöneich, A. G., Laurence, S. J., Sullivan, B. T., Bodony, D. J., Freydin, M., Dowell, E. H., and Buck, G. M., "Hypersonic Fluid–Structure Interactions in Compression Corner Shock-Wave/Boundary-Layer Interaction," *AIAA Journal*, Vol. 58, No. 9, 2020, pp. 4090–4105. https://doi.org/10.2514/1.J059152

54. Schöneich, A. G., Whalen, T. J., Laurence, S. J., Sullivan, B. T., Bodony, D. J., Freydin, M., Dowell, E. H., Stacey, L. J., and Buck, G. M., "Fluid-Thermal-Structural Interactions in Ramp-Induced Shock-Wave Boundary-Layer Interactions at Mach 6," AIAA Paper 2021-0912, *AIAA SciTech 2021 Forum*, Virtual Event, 11-5 & 19-21 January 2021. https://doi.org/10.2514/6.2021-0912

55. Hoffman, E. N. A., Rodriguez, J. M., Cottier, S. M., Comb, C. S., Bathel, B. F., Weisberger, J. M., Jones, S. B., Schmisser, J. D. and Kreth, P. A., "Model Analysis of Cylinder-Induced Transitional Shock-Wave / Boundary-Layer Interaction Unsteadiness," *AIAA Journal*, Vol. 60, No. 5, May 2022, pp. 2730-2048. https://doi.org/10.2514/1.J060880

56. Lum, J. S., Keene, L. T., Goldberg, B. M., Busby, E., Rousso, A. C., Bathel, B. F., Weisberger, J. M., Buck, G. M., Stobbe, D. M., and Stolken, J. S., "In-Situ Optical Detection for Ultrasonic Characterization of Materials in a Mach 10 Hypersonic Wind Tunnel," Phys. Rev. Applied 18, 044062 – Published 26 October 2022 https://journals.aps.org/prapplied/abstract/10.1103/PhysRevApplied.18.044062

57. Keene, L. T., Lum, J. S., Busby, E., Rousso, A. C., Goldberg, B. M., Buck, G. M., and Stolken, J. S., "Laser Speckle Pattern Stability in Hypersonic Regimes for Experimental Mechanics and Metrological Studies," *Journal for the Society for Experimental Mechanics: Experimental Techniques*, Submitted January 2023 - to be published.

58. Rodrigues, N. S., Tyrrell, O. K., Danehy, P. M., Rieken, E. F., Hollis, B. R., Ripley, W. H., Crider, J. B., Robbins, A. W., Reynolds, T., and Wright, S. A., "Application of PLIF to Investigate the Hypersonic Wake of a LOFTID-Relevant Model at Mach 10," NASA/TM–20240000817, April 2024.

59. Danehy, P. M., Bathel, B. F., Rodrigues, N. S., Inman, J., and Johansen, C. T., "Review of planar laser-induced fluorescence measurements in the NASA Langley 31-Inch Mach 10 Air Tunnel," AIAA Paper 2024-1314, *AIAA SciTech 2024 Forum*, Orlando, FL, 8-12 January 2024. https://doi.org/10.2514/6.2024-1314

60. Rodrigues, N. S., Tyrrell, O. K., Rieken, E., Hollis, B. R., and Danehy, P. M., "FLEET and PLIF velocimetry within a Mach 10 hypersonic air flow," AIAA Paper 2024-2323, *AIAA SciTech 2024 Forum*, 8-12 January 2024. https://doi.org/10.2514/6.2024-2323

61. Rodrigues, N. S., Bathel, B. F., Danehy P. M., "A Comparison of NO Laser-Induced Fluorescence Models at Conditions Relevant to Supersonic and Hypersonic Flows," AIAA Paper 2022-0897, *AIAA SciTech 2022 Forum*, San Diego, CA, 3-7 January 2022. https://doi.org/10.2514/6.2022-0897

62. Multiline molecular tagging velocimetry of nitric oxide at 100 kHz using an injection-seeded burst-mode OPO (https://opg.optica.org/ao/viewmedia.cfm?uri=ao-63-5-1247&html=true)

63. Long-lived nitric oxide molecular tagging velocimetry with 1 + 1 REMPI (https://opg.optica.org/viewmedia.cfm?r=1&rwjcode=ol&uri=ol-49-5-1297&html=true)

64. Rodrigues, N. S., Danehy P. M., Jiang, N., Hsu, P., Leicht, J., and Roy, S., "100 kHz High-Spectral-Resolution NO-PLIF Measurements for Compressible Flows," AIAA Paper 2023-0405, *AIAA SciTech 2023 Forum*, 23-27 January 2023. https://doi.org/10.2514/6.2023-0405

65. Danehy, P. M., Burns, R. A., Reese, D. T., Retter, J. E., and Kearney, S. P., "FLEET Velocimetry for Aerodynamics," *Annual Review of Fluid Mechanics*, Vol. 54, No. 1, 2022, pp. 525-553.

66. Chou, A., Leidy, A., King, R. A., Bathel, B. F., and Herring, G., "Measurements of freestream fluctuations in the NASA Langley 20-Inch Mach 6 tunnel," AIAA Paper 2018-3073, *Fluid Dynamics Conference*, June 25-29, June 2018. https://doi.org/10.2514/6.2018-3073

67. Bathel, B. F., Herring, G. C., Weisberger, J. M., Chou, A., and Jones, S. B., "Simultaneous focused laser differential interferometry and high-speed schlieren in a Mach 6 flow," *Measurement Science and Technology*, Vol. 32, No. 9, June 2021.

68. Rhode, M.N. and DeLoach R., "Hypersonic Wind Tunnel Calibration Using the Modern Design of Experiments," AIAA Paper 2005-4274, 41st AIAA/ASME/SAE/ASEE Joint Propulsion Conference & Exhibit, Tucson, AZ, 10-13 July 2005. https://doi.org/10.2514/6.2005-4274

69. Fay, J. A., and Riddell, F. R., "Theory of Stagnation Point Heat Transfer in Dissociated Air," *Journal of the Aeronautical Sciences*, Vol. 25, No. 2, February 1958, pp. 73–85, 121. https://doi.org/10.2514/8.7517